By

NEST – NanoEngineering, Science and Technology

CHSLT – Center for Holographic Studies and Laser micro-mechaTronics

Mechanical Engineering Department

Worcester Polytechnic Institute

Worcester, MA 01609-2280

Abstract

The conventional methods for diagnosing pathological conditions of the tympanic membrane (TM) and other abnormalities require measuring its motion to an acoustic excitation for its use in a clinical environment. To obtain comprehensive quantitative diagnostic information from the motion of the entire surface of the TM, it is necessary to devise an integrated system capable to induce an acoustic stimulus and accurately recording the motion. To accomplish this goal, a sound presentation system (SPS) capable of producing acoustic stimuli in the frequency range of 25 Hz to 8 kHz at known amplitudes is synthesized in this thesis. This system is then integrated with optoelectronic holographic system (OEHO) that utilizes laser interferometry to record and reconstruct phase shifted images with the help of a digital camera. The OEHO is capable of accurately recording nanometer scale motion of the TM.

The preliminary design of the SPS depends on the physical dimensions of the human ear, such as the diameter of the TM 8-10 mm, depth of the ear canal (about 30 mm), and also dimensions of the OEHO system such as: diameter of tip of the otoscope head for optical access (8 mm), and possible locations for integration with the OEHO. The characteristics of the system are based on the intensity of the acoustic stimulus necessary to vibrate the TM 90-110 dB SPL, and method of producing stimuli.

To accomplish this goal, the nature of sound wave propagation through a circular pipe with known dimensions is analyzed analytically, experimentally, and by using finite element analysis (FEA). The pipe is further investigated for optimum parameters using FEA by introducing changes in the diameter (3.8 mm, 6 mm, 10 mm), length of the pipe (30 mm, 60 mm, 90 mm), radius of the curvature (50 mm, 75 mm, 100 mm), and strength of the sound power source

(0.2 W, 0.4 W, 0.6 W). The comparative results provide guidelines for the design of the first version of the SPS (SPS_V1).

The SPS_V1 consists of a symmetric design to produce the acoustic stimulus at the TM and a microphone to measure the sound pressure at the TM. The system is capable of housing a range of speakers from 2 mm to 15 mm in diameter. The SPS_V1 can directly interface with the standard medical speculums used for human ear testing. Also, the system is capable of interfacing with all available versions of the OEHO. The SPS_V1 is currently being evaluated in a medical-research environment to address basic otological questions regarding TM function. The performance characterization of the system inside an artificial ear canal with two different speaker configurations is herein shown, and the potential improvements and utilization are discussed.

The thesis is dedicated proudly to my family.

Acknowledgements

At this time, it is extremely important to extend my gratitude to a number of individuals and organizations which have aided me and made it possible for me to arrive at this moment with these results.

Most important, I'm very grateful for all the support and friendship which were offered to me by my advisor Professor Cosme Furlong, whose contribution in my student life is instrumental and whom I shall never forget. The thesis committee has demonstrated unwavering support during my Thesis research. The Center for Holographic Studies and Laser micromechaTronics (CHSLT) in the WPI Mechanical Engineering Department, for the use of both their facilities and equipment, deserves much praise and recognition.

I wish to acknowledge the assistance of Professor John J. Rosowski, Mike Ravicz, Dr. Jeffrey T. Cheng for their collaboration, advice and suggestions in my experimental work. Funding and support from Massachusetts Eye and Infirmary for the use of their facility and equipment for my experimental work.

Accolades are also extended to Dr. Mauricio Flores, Ellery Harrington, Ivo Dobrev, Weina Lu, Peter Hefti from the CHSLT laboratories for their enduring support and invaluable assistance.

Finally, I want to thank my dear family for their love and unending support throughout my tenure. Without them I would not have been able to accomplish anything.

Table of Contents

List of figures

Nomenclature

Z	acoustic impedance
S	Surface area (m^2)
I	acoustic intensity
υ	particle velocity
P	normalized sound pressure
p	sound pressure (Pa)
p_i	instantaneous sound pressure
v_i	instantaneous particle velocity
a	radius of the pipe
L	length of the pipe
t	wall thickness
r	radial cylindrical co-ordinate
ψ	angular cylindrical co-ordinate
z	axial cylindrical co-ordinate
$\varphi(t,r)$	velocity potential (m^2/s)
C_s	speed of sound (m/s)
f	frequency in Hz.
ω	angular frequency (rad/sec)
FR_{ref}	frequency response at reference point
FR_{exp}	frequency response at a point under experimentation
p	acoustic pressure (N/m^2)
p_0	reference acoustic pressure (N/m^2)
q	dipole source (N/m^3)
ρ_0	air density (kg/m^3)
(ξ, η)	coordinates of hologram plane

(x, y)	Cartesian coordinates of the reconstructed image
$a\,(\xi, \eta)$	complex amplitude distribution on the hologram plane
$a'_n(\xi, \eta)$	complex amplitude distribution at different observation planes
a_n	represents an external source term.
$\mathcal{B}$	adiabatic bulk modulus
TM	tympanic membrane
SPS	Sound Presentation System
FEA	Finite Element Analysis
OH	Otoscope Head
LDV	Laser Doppler Vibrometer
SLV	Scanning Laser Vibrometer
BS	Beam Splitter Cube
PMF	Polarize Maintaining Fiber
$\Omega(x, y)$	fringe-locus function
k	wave number
$SPL_{(freq\_range)}$	sound pressure level reading for omplete frequency response
$SPL_{(freq\_ref)}$	sound pressure level reading for reference frequency value
$FR_{(ref)}$	frequency response at reference location
$FR_{(exp)}$	frequency response at specific location under experimentation
λ	wavelength of laser light
J_n	nth- order Bessel function of first kind
Y_n	nth- order Bessel function of second kind
k_r	propagation vector component of wave number in radial direction
k_z	propagation vector component of wave number in axial direction
$\boldsymbol{u}(t, r)$	time – harmonic acoustic fluid velocity vector
$\hat{n}$	unit vector normal to the inside surface of the pipe (analytical)
n_s	unit vector normal to the inside surface of the pipe (computational)

Objectives

The objectives of this Thesis are development and testing of the sound presentation system (SPS) for loading of the tympanic membrane (TM) and integration of the SPS with the optoelectronic holographic otoscope (OEHO) to provide complete package for diagnosing the human TM in the clinical environment.

1. Introduction

The rapid growth of the precise medical equipment industry has led to the development and use of even more accurate and sophisticated medical tools. Diagnosis and treatment of human ear disorders is a challenging field and significant research and development activities in this field have led to examination of the tympanic membrane (TM) than ever before.

The TM, which plays an important role in the transmission of sound into the cochlea, is a tissue separating the external ear canal from the middle-ear cavity [Rosowski et al. 1996]. Experimental measurements and theoretical analysis have been done to study the structure [Lim, 1995], mechanical properties [Funnel and Laszlo, 1978; Fay et al., 2005] and acoustic function [Tonndorf and Khanna, 1970; Khanna and Tonndorf, 1972; Rosowski et al., 1989] of the TM.

The efficiency of sound coupling through the TM can be hindered by changes to the TM through trauma or middle-ear diseases. Measurement of TM deformation for different acoustic stimuli can provide information about the degree of hearing losses [Hulli, 2008].

There are different approaches used to perform the diagnostic procedures on the mobility of the entire TM to acoustic stimuli, e.g., multi or single frequency tympanometry [Shanks et al., 1988; Margolis et al., 1999], ear canal reflectance or power absorption [Keefe et al., 1993; Feeney et al., 2003; Allen et al., 2005], and static pressure induced variations in sound pressure [Wada et al., 1989; Wada et al., 2002]. We are developing a full-field-of-view measurement technique to quantify the motion of the entire surface of the TM. Developments are based on principles of Optoelectronic holography, which has been successfully tested in many applications and environments, [Pryputniewicz et al., 2002; Furlong and Pryputniewicz, 1998; Powell and

Stetson, 1965] and have shown the capability to provide the desired information on the state of the TM.

In order to implement the full-field-of-view measurement technique, there is need of a system, that will acoustically excite the sample at known frequencies and amplitudes. Development of such a system is synthesized in this thesis.

The developed acoustic system carries the sound signal towards the tympanic membrane at specified frequencies and amplitudes. To achieve this, waveguides with optimum dimensions based on structural and fluid flow constraints are analyzed. Initially, the propagation of sound waves through a waveguide of circular cross section is studied and verified analytically, computationally, and experimentally. After verifying computational simulation tools and experimental procedures, a series of waveguides are studied and simulated by varying the cross section, length to diameter ratio, radius of curvature, sound source strength, and surrounding domain size. Knowledge gathered from all the simulations is used to propose the first version of the sound presentation system (SPS_V1). The proposed design has substantial wall thickness to appropriately mount the speaker and avoid its vibration, an aperture for optical access, a fixture to hold the speaker, and a specific position to locate the microphone. Also, the first version of the SPS_V1 can be directly integrated to all packaged versions of the optoelectronic holographic otoscope (OEHO) systems being developed. Next, the full system simulation of SPS_V1 is carried out and the SPS_V1 is manufactured using rapid prototype processes. Extensive testing is carried out on the SPS_V1 for disturbances in the optical characteristics of the OEHO system, sound pressure level (SPL) recorded with ideally sealed ear canal and partially open ear canal, SPL recorded with different sound sources, and the effect on SPL due to acoustically sealing the optical path [Ravicz et al., 2007].

This synthesis provides concrete information for further optimization of the SPS to be finally implemented in the clinical environment.

2. Anatomy of the ear

Anatomically, the mammalian ear can be divided into three functional parts as shown in Fig. 2.1: the outer (external) ear, the middle-ear and the inner ear. The external ear, which consists of auricle or pinna (the visible part of the ear) and the external auditory canal collects sound waves and transmits them to the middle-ear.

The middle-ear is a space filled with air that encapsulates the three middle-ear bones (ossicles) and the middle ear muscles, as presented in Fig. 2.2. The first bone, the hammer (malleus), is connected to the anvil (incus), which in turn is connected to the stirrup (stapes). The middle-ear is attached to the back of the nose (nasopharynx) by the Eustachian tube. The sound energy coming from the outer ear causes the TM to vibrate. The tympanic membrane transforms acoustic energy to mechanical energy in the form of ossicular motion. The steps convert mechanical energy to acoustic energy within the inner ear.

The inner ear contains the semicircular canals and the other vestibule for balance, as well as the cochlea for hearing. It is in the inner ear where the acoustic disturbance related to sound is transformed into neural action potentials via the vibration of microscopic hairs (the stereocilia) with varied lengths that are attached to sensory cells. The hair cells are arranged in an orderly fashion along the length of the auditory inner ear, where those that respond to lower frequencies are farther from the stapes. This tonotopic mapping allows the coding of sound frequency and the perception of pitch.

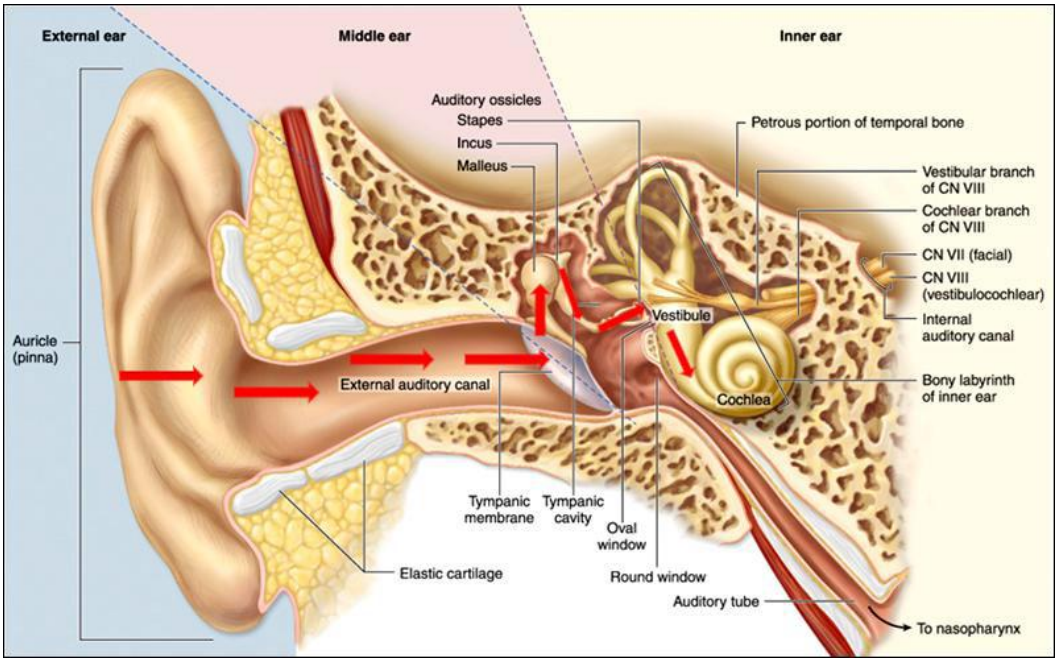

Fig. 2.1. Anatomy of the human ear: The cross section of human ear showing divisions of the outer, middle, and inner ears [Wikipedia, 2011].

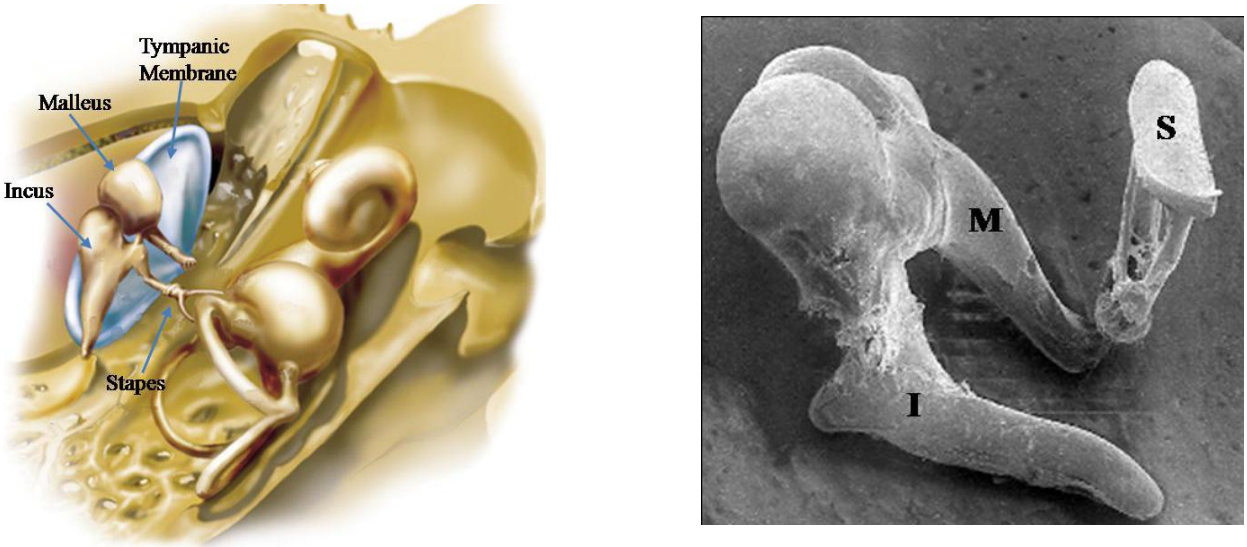

(a) (b)

Fig. 2.2. Middle-ear ossicles: (a) chain of ossicles and their ligaments; (b) the three middle-ear bones: malleus (M), incus (I), and stapes (S) [Csillag, 2005].

2.1. The tympanic membrane

The tympanic membrane is a semi-transparent, thin, cone shaped membrane, which is the boundary between the outer and the middle-ear, as shown in Fig. 2.3

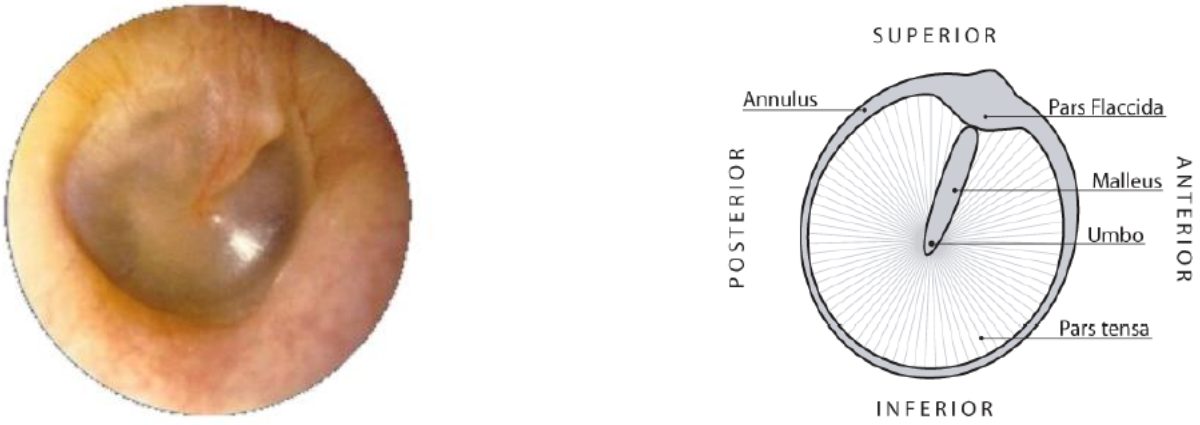

(a) (b)

Fig. 2.3. Structure of human tympanic membrane: (a) normal tympanic membrane as seen through an otoscope [Grundman and Wigton, 2008]; (b) schematic of a right tympanic membrane [Sundberg, 2008].

The TM is composed, structurally, of three layers. The lateral (or outside) layer is a skin-like epidermis; the medial (or inside) layer is mucosal lining much like the lining of the mouth and nose. In between is a fiber rich connective layer, called the lamina propria [Sanna et al., 2003]. The diameter of the TM is 5-10 mm, and the depth of cone is about 1.5 mm [Dirckx and Dcraemer, 2000]. The exterior edge of the TM, named the annulus, or the annular ring, consists of a fibrous and cartilaginous tissue that is both thicker and stiffer than the rest of the membrane [Sundberg, 2008]. The TM is between 55 and 140 micrometers thick [Kuypers et al., 2006]; it is thinnest in the central parts of the posterosuperior quadrant and thickest in the vicinity of the inferior part of the annulus. The triangular extension at the superior part of the TM is the flexible *pars flaccida*. The *flaccida* is about 10% of the area of the TM, and moves

independently from the rest of the TM area, the *pars tensa*, that is tightly coupled to the ossicular chain [Sundberg, 2008]. Anatomical and physical features of the TM are ideally suited for the sound transmission in varying frequency ranges hence analyzing TM motion has proven to be helpful in the diagnosis of middle ear disorders [Rosowski, et al., 2008].

2.2. Medical techniques and procedures for diagnosis

To diagnose any unhealthy conditions of the middle-ear, there are a limited number of different methods practiced. Developed by clinicians, tympanometry, Fig. 2.4, is a measure of the mobility of the TM and middle-ear and depends on the status of the TM, the middle-ear air space, and the ossicular chain [Schubert, 1980; Mikoklai et al., 2008]. Tympanometry is routinely used to help detect the presence of fluid in the middle-ear and TM perforations, but is less useful in the diagnosis of ossicular disorders.

A tympanogram is a graphical representation of the relationship between air pressure in the external canal and the impedance of the tympanic membrane and the middle-ear system [Mikoklai et al., 2008]. Acoustics impedance is inversely related to the mobility of the tympanic membrane; it is mobility that physicians are testing when they determine the health of a patient's tympanic membrane [Schubert, 1980]. The physics of transmitting sound is much like what happens when a drum is struck: part of the sound is reflected while the other part is absorbed by the instrument itself. Likewise, when the tympanic membrane is hit by a sound, some of the sound waves are absorbed and sent to the inner ear by the ossicles, while the remaining part of the sound is reflected back.

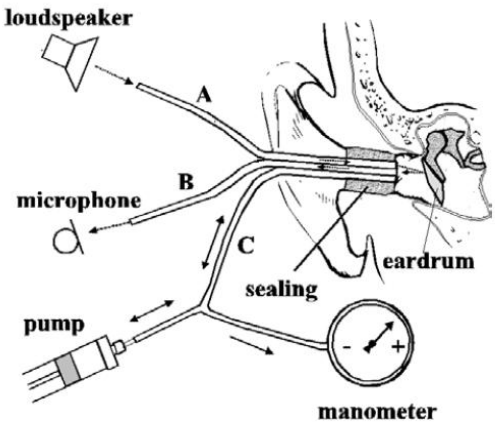

Fig. 2.4. The tympanometer consists of a hand-held probe to be inserted into the ear. The probe is composed of three tubes containing a loudspeaker, a microphone, and a pump [Mikoklai et al., 2008].

Abnormal TM mobility is an indication of a conductive hearing loss: a problem with how sound is conducted to the inner ear sensory mechanism. A sensory or neural hearing loss describes a pathology associated with the conversion of sound energy into electrical energy within the hair cells and the conduction of these electrical sensory signals to the brain. The sensory or neural hearing losses are differentiated from conductive pathologies via the use of bone-conduction hearing test. In bone-conduction testing, sound is presented to the inner ear via a mechanical vibrator placed firmly on the skull. The bone-conducted sound is thought to bypass the middle-ear and stimulate the inner ear directly. A person with a loss of sensitivity to air-conducted sound and normal sensitivity to bone-conducted sound is thought to have a conductive hearing loss related to either middle or external-ear pathology.

Physicians induce different pressures in the ear canal and take measurements with relation to the acoustic compliance of the air volume in the enclosed ear canal [Schubert, 1980]. If the recorded volumes are found to be different from that of the normal ear, then it is very likely that

there is a problem in the middle ear [Schubert, 1980]. The type of pattern detected can also help to determine what type of middle-ear condition the patient has, enabling physicians to determine the method of treatment [Katz, 1994]. This type of analysis, together with the use of an otoscope, provides the information necessary to make proper diagnoses of specific ear ailments [Katz, 1994]. This type of testing requires various kinds of expertise and a large commitment of time.

A noncontact system that uses Laser Doppler Vibrometers (LDV) to map tympanic response is one of a newest experimental method to test the tympanic membrane. First, the device ascertains and reports the velocity of surfaces in a system and then extracts relevant data for use by audiologists [Castellini et al., 2006, Rosowski et al., 2008]. These measurements have been demonstrated to be sensitive to several middle-ear pathologies including TM perforations and ossicular fixations and interruptions. When applied to a sample, the LDV supplies point-by-point information [Rosowski et al., 2008]. LDV can be used to measure vibrations in order to collect multiple data points at a time and receive a magnified "field-of-view" of their data.
Used in combination with a Scanning Laser Vibrometer (SLV) to collect data from multiple points on a sample simultaneously, points within a minute area for example, to provide the whole image of the samples response [Castellini et al., 1998]

There are other methods that have the capability to provide data on the TM response to be used for further analysis. Holographic interferometry, as an optical testing method, is helpful in analysis of sample deformation in full-field-of-view [Furlong and Pryputniewicz, 1998; Furlong et al., 2002; Furlong et al., 2008; Hulli, 2008; Hernandez-Montes et al., 2008]. It must be remembered that single point measurements are not sufficient to characterize the motion of the entire TM. Special analysis equipment is required for full-field-of-view measurement

methodologies of nanometer resolution if comprehensive data about the tympanic membrane is to be provided.

Optoelectronic holographic interferometry is one of the current areas of laser-related research capable of providing physicians with desired information on the condition of tympanic membranes [Furlong et al., 2008]. An overview of the optoelectronic holographic otoscope (OEHO) that we are developing for diagnosis of the TM is provided in the following Section.

3. Optoelectronic holographic otoscope (OEHO) system

To obtain comprehensive quantitative diagnostic information from the motion of the entire surface of the TM, it is necessary to devise an integrated system capable of accurately recording the motion due to induced acoustic stimulus. Figure 3.1 shows a diagram of such a system, which contains fiber optic subsystem, otoscope head (OH) subsystem, and SPS.

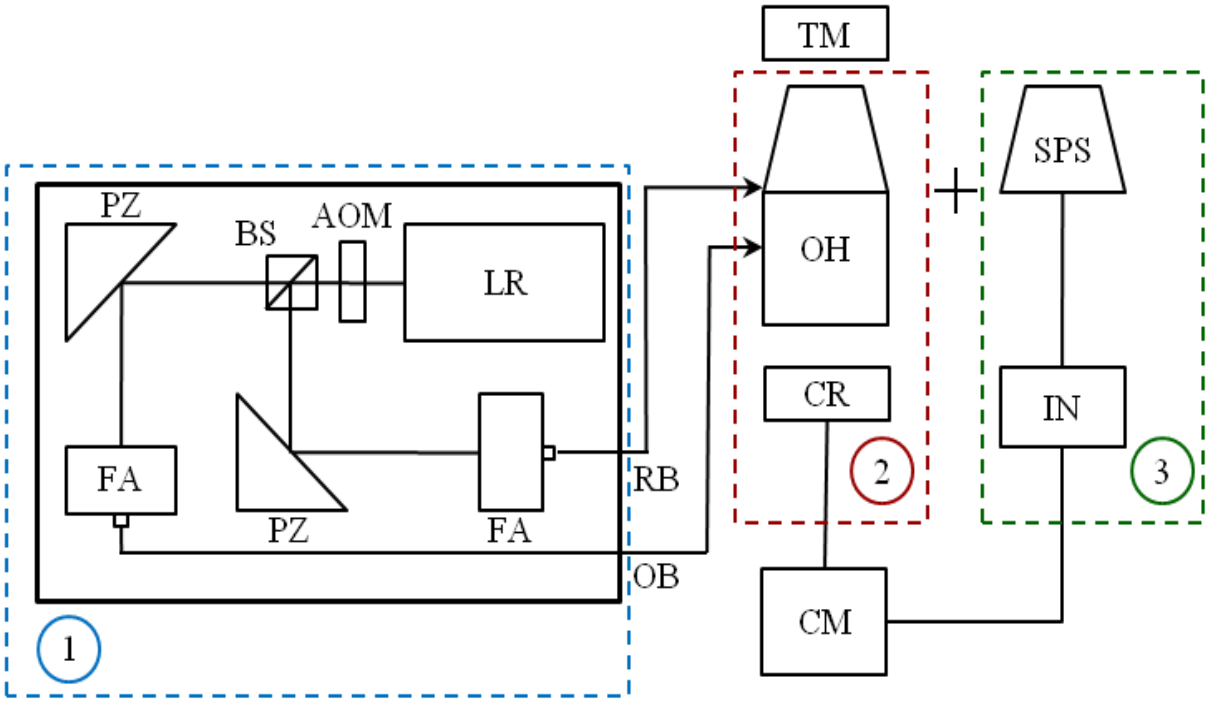

Fig. 3.1. Schematic diagram of OEHO system: tympanic membrane (TM) is the sample under investigation; fiber optic subsystem (1), otoscope head subsystem (2), sound presentation system (SPS) (3); 532nm, 20mW green laser(LR), Acousto-optic modulator (AOM), Beam splitter (BS), Piezoelectric positioners (PZ), laser to fiber coupler assembly (FA), Reference beam(RB), Object beam (OB), image processing computer (CM), high-speed digital camera (CR), Optical head (OH), Acoustic signal input (IN).

3.1. Fiber optic subsystem

Figure 3.2 depicts the fabricated fiber optic subsystem, containing a 532nm wavelength laser (LR) with 50 mW of power. The laser is mounted on a heat sink to avoid degradation due to overheating. The laser beam initially passes through an AOM that enables stroboscopic illumination. At the exit of the AOM, a beam splitter cube (BS) is mounted, which splits the laser beam with an 80% transmission, 20% reflection ratio. Separated laser beams are reflected from respective piezoelectric mirrors (PZ) towards the laser to fiber coupler assemblies (FA). Piezoelectric mirrors (PZ) are used for accurately reflecting the laser beam towards the FA. PZ can also be controlled with the computer to achieve nanoscale displacements for the purpose of phase shifting the laser beam.

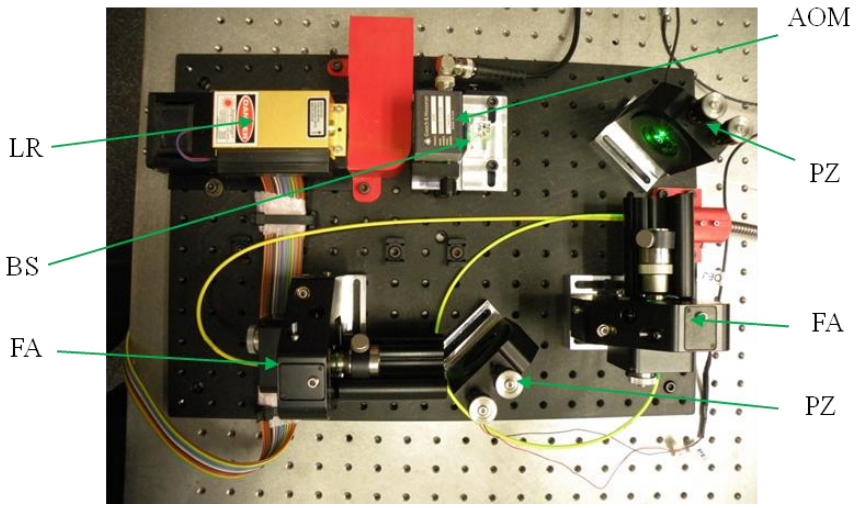

Fig. 3.2. Fabricated fiber optic subsystem; beam splitter (BS), acousto-optic modulator (AOM), 50 mW, 532 nm wavelength laser (LR), piezoelectric positioners (PZ), laser to fiber coupler assembly (FA).

After the laser output is split by the BS in two beams, defined as object beam for transmission and reference beam for reflection, these beams are reflected from PZ assemblies towards FA assemblies. The FA assemblies are used for coupling laser light into the core of polarization

maintaining fibers (PMFs). Each FA assembly has 3-axial degrees and one rotational degree of freedom to achieve high coupling efficiency. The coupling efficiency is defined as

$$Coupling\ efficiency = \frac{Power\ coupled\ into\ the\ optic\ fiber}{Laser\ beam\ power\ before\ the\ coupling} \quad (3.1)$$

The FA assembly produces about a 60% of coupling efficiency between the incident light and optical fiber core. Thereafter, these optical fibers (object beam and reference beam) carry the laser light to the OH subsystem.

The PMFs used in this setup are designed for operating wavelength range of 400-600 nm consistent with the wavelength of the laser used in this setup. As the name depicts, these optic fibers possess the characteristic of preserving the polarization of the laser light during the propagation, which add mechanical stability to the OEHO system.

The design principle of such fibers is based on inducing stress in the core of the fiber with the help of non-circular cladding cross-section or via rods of different material.

As OEHO system is designed for measuring nanometer scale deformations of the TM, the stability of the optic fiber proves vital. Immunity of the PMF's to bends, twists, and environmental changes, are useful for coherent optical transmission systems. Therefore, panda type PMF is used in this setup. The laser light is focused into the slow axis of the PMF with the help of FA assemblies.

3.2. Otoscope head (OH) subsystem

Conventional holographic interferometers use lenses to focus an image onto the detector of the camera. Another holographic technique that allows focusing of images by software using numerical reconstruction algorithms instead of lenses is lensless digital holography [Kreis, 2005]. Figure 3.3 shows a packaged version of the otoscope head (OH) subsystem based on digital holography technique with numerical reconstruction.

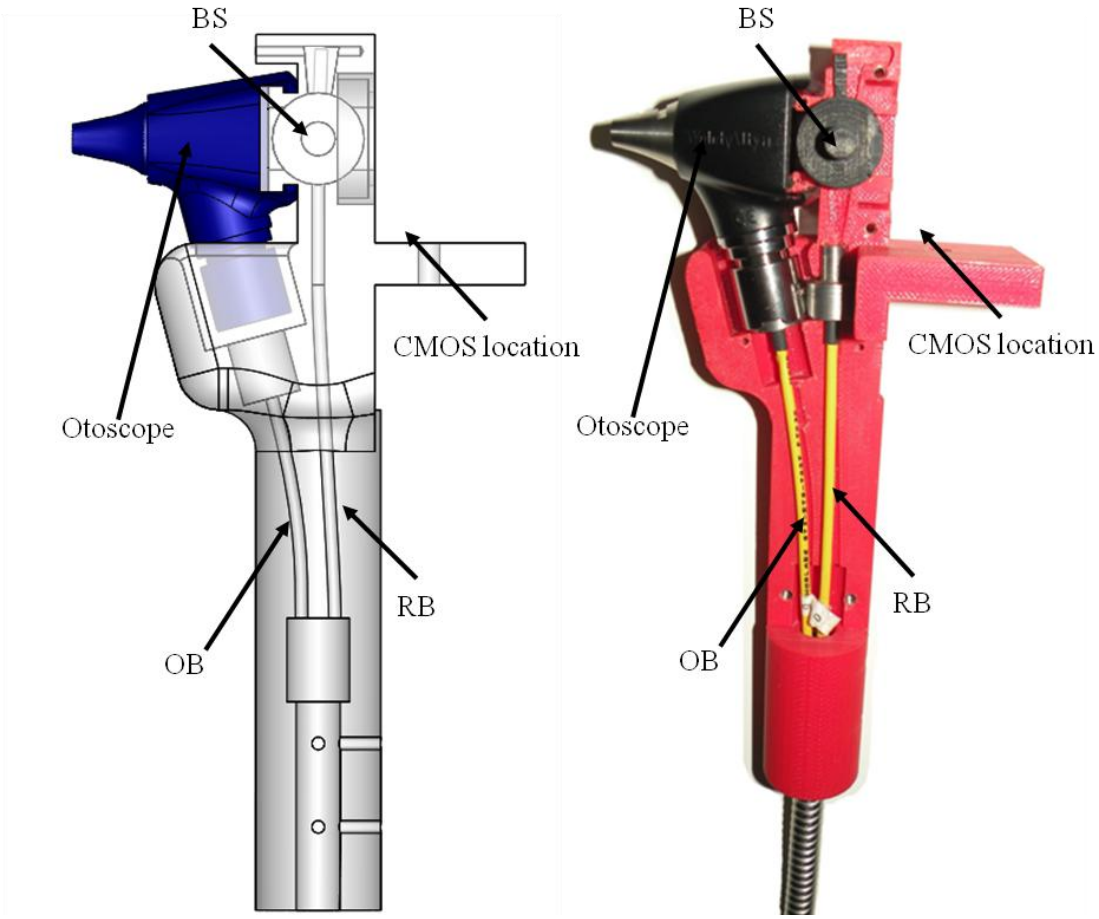

(a) (b)

Fig. 3.3. Lensless OH configuration: (a) CAD model of OH system; (b) Fabricated model of OH; high speed digital camera (CMOS), beam splitter (BS), reference beam (RB), object beam (OB).

The CMOS camera records the hologram formed by the interference of the object beam and the reference beam. The recorded images contain amplitude and phase information. Holographic phase stepping interferometry is used to obtain phase change in the backscattered light from the object when it is exposed to an external excitation (mechanical, electrical, thermal etc.) that induces a physical change in its structure [Kreis, 2005].

3.3. Working of otoscope head (OH) subsystem

Numerically reconstructing an image with the OEHO is based on phase stepping digital holography method. Similar to classical holography, the digital holography uses superposition of the object and reference beams to create a hologram containing optical information related to shape and deformation.

In digital holography the holograms are projected on an imaging sensor, which allows for the digital recording and analysis of the image information. The specific characteristic of this technique, based on the recording full fields of intensity and phase of the light scattered by the object, allows the intensity and phase information on any plane along the light propagation direction to be numerically reconstructed. This property allows for the recording of holograms without any optical elements, thus reconstructing the object image purely numerically with the help of a computer [Kries, 2005]. The recorded images are of the form

$$I_n(u,v) = I_o(u,v) + I_r(u,v) + 2A_o(u,v)A_r(u,v)\cos[\Delta\phi(u,v) + \theta_n], \quad (3.2)$$

where I_o and I_r are the object and reference beam intensities as a function of pixel coordinates (u, v), which are the square of the object and reference beam amplitudes A_o and A_r, respectively, $\Delta\phi$ is the random phase, and the finite known phase step increments are θ_n. For every

reconstructed image, the OEHO records four images containing holographic patterns that result from the phase shifting of the reference beam (RB) in steps of multiples of $\theta_n = \frac{\pi}{2}$.

$$I_1 = I_o + I_r + 2A_oA_r \cos[\Delta\phi + 0], \tag{3.3}$$

$$I_2 = I_o + I_r + 2A_oA_r \cos\left[\Delta\phi + \frac{\pi}{2}\right], \tag{3.4}$$

$$I_3 = I_o + I_r + 2A_oA_r \cos[\Delta\phi + \pi], \tag{3.5}$$

$$I_4 = I_o + I_r + 2A_oA_r \cos\left[\Delta\phi + \frac{3\pi}{2}\right], \tag{3.6}$$

The recorded images are then processed in a digital reconstruction process using four-step algorithm. The recorded reconstructed image consists of a complex light distribution data array containing amplitude and phase information that can be expressed as

$$a(\xi,\eta) = (I_1 - I_3) + i(I_4 + I_2) \tag{3.7}$$

where I_n represent the stored images in the object plane at each step of the phase shifting.

Intensity and phase distributions at various planes are reconstructed using the result of the Rayleigh-Sommerfeld diffraction integral for various distances away from the imaging sensor. The reconstruction is used to derive expressions of the spectral irradiance and radiant intensity on the observation plane. The Rayleigh-Sommerfeld integral is defined as follows [Kries, 2005].

$$a'(x,y) = \frac{1}{i\lambda} \iint a(\xi,\eta)\, \frac{1}{r}\, e^{-ikr} \cos\Theta \; d\xi d\eta \tag{3.8}$$

where $a'(x,y)$ is the propagated and reconstructed wave field on the observation plane, which is the hologram formed by the interference of reference and object beams, r is the magnitude of the vector from the object to the observation plane, Θ is the angle between the normal of the observation plane and the vectorr, λ is the wavelength of the laser light, k is the optical wave number and is equal to $\frac{2\pi}{\lambda}$. The value of r is

$$r = \sqrt{(x-\xi)^2 + (y-\eta)^2 + d}. \tag{3.9}$$

The key parameter here is d, which is the distance between the image sensor and the reconstruction plane. This is analogous to finding the focal plane of an image using a lens system. This behavior is explained in Fig.3.4, where the best reconstructed image corresponds to the reconstruction plane.

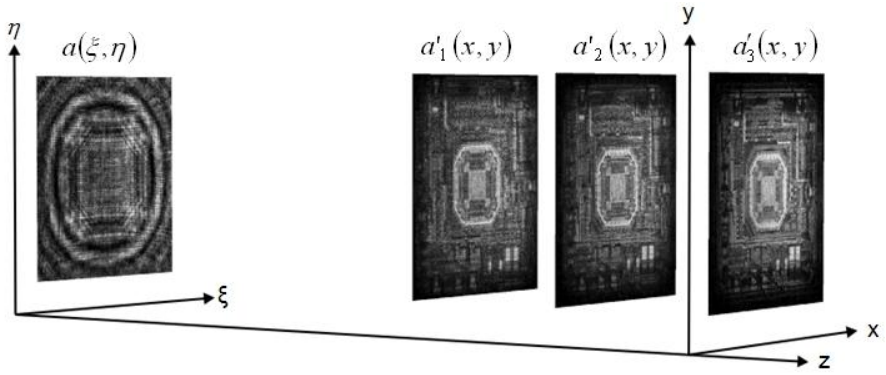

Fig. 3.4. Reconstruction distance in the plane image.

In order to measure deformations much less than $\frac{\lambda}{2}$ in magnitude, a double exposure stroboscopic mode is implemented in the OEHO. In order to measure the phase changes, the information of the reference and deformed state of the object are read individually. Because of the fact that the reconstructed hologram image is a complex data array, the imaginary and real part can be used to extract the phase information. This is done by using the fact that the real part of the reference and the real part of the deformed state are contained in the denominator (real part) of the $arctan$ function before and after of the phase change. Similarly, the imaginary part of the reference and deformed state are contained in the imaginary part or numerator of the $arctan$ function. The real and images are processed to obtain the optical phase as follows,

$$\varphi'^{(x,y)} = arctan\left[\frac{a_2'(x,y) * a_3'(x,y) - a_1'(x,y) * a_4'(x,y)}{a_2'(x,y) * a_4'(x,y) + a_1'(x,y) * a_3'(x,y)}\right], \tag{3.10}$$

where $a_1'(x,y), a_2'(x,y)$ represents the real and the imaginary part of the reference state, meanwhile $a_3'(x,y), a_4'(x,y)$ are the real and imaginary part of the deformed state. Each pair of these reconstructed holograms is calculated in turn by four phase stepped images used in the reconstruction algorithm.

3.4. Time-averaged mode

In time-averaged mode, measurements are obtained by continuous image acquisition and exposure of the camera to display intensity distributions of the form

$$I(x,y) = \frac{1}{\Delta t}\int_{t}^{t+\Delta t} I_t(x,y,t)dt. \tag{3.11}$$

Time-Averaged mode allows for the viewing of the near-instantaneous movement of an object. This is accomplished by using a time varying fringe-locus function, $\Omega(x,y)$ related to the vibrating object [Pryputniewicz, 1985, 1987, 1989].

Images recorded contain information about the amplitude of an object's vibration in the form of fringes. Every set of reconstructed images consists of four holograms recorded using a phase stepping technique, where the reference beams phase is controlled by a stepping function synchronized with the acquisition rate of the camera. The fringes obtained are contours of equal vibration amplitudes of the spatial vibration modes corresponding to the zeros of the square of the zero-order Bessel function of the first kind. This technique is also known as the real time holography technique [Powell and Stetson 1965; Kries, 2005].

3.5. Stroboscopic mode

In stroboscopic mode, quantitative measurements are obtained by measuring *Ω(x,y),* corresponding to varied state of deformation. The phase difference,

$$\Delta\Omega(x,y) = \Omega_{i+1}(x,y) - \Omega_i(x,y), \tag{3.12}$$

provides a direct measurement of relative deformations between two states of interests, i, and $i+1$.

In this mode, recording the holograms by using a series of short laser pulses is exercised. Initially, a reference state of the target under investigation is recorded. Next, short laser light pulses are synchronized with the excitation signal given to the test object, as shown in Fig. 3.5. This enables recording the displacement of the object at a specific location in its excitation. [Furlong et al, 2008].

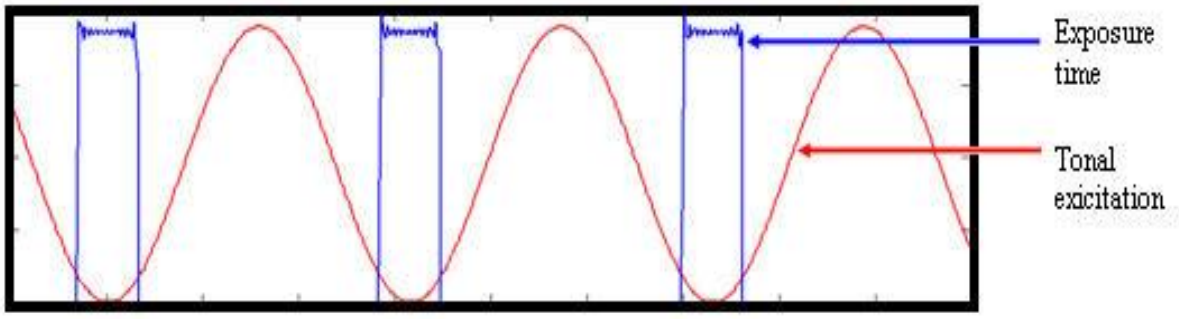

Fig. 3.5. Stroboscopic mode: illumination synchronization with object excitation.

4. Approach to SPS synthesis

To design a system capable of generating the acoustic stimulus at known frequency and amplitude, it is necessary to scrutinize the effect of each parameter involved in the system design. Pipes of different cross sections and lengths are used to carry the acoustic stimulus. Before investigating the effects of geometrical changes on the capability to carry the acoustic signal, it is necessary to validate the methods used for the analysis. To achieve this, an acrylic pipe open at one end, with a point sound source at the center of the closed surface is studied analytically, simulated computationally, and finally validated experimentally. Upon validation of computational tools, the geometrical parameters of the pipe are varied and simulated computationally. The effects of parametric investigation are observed by plotting frequency response of each variation in the range of 25 Hz to 8 kHz. From the simulations, the best suitable combination is selected. A computational simulation of the selected combination is performed. Necessary design modifications are done to integrate the system with the otoscope head (OH) subsystem, and also fulfill the design objectives set at the start of the system design. Finally the manufactured system is calibrated and made available to use with the OEHO system. Flow chart of the approach is depicted in Fig. 4.1.

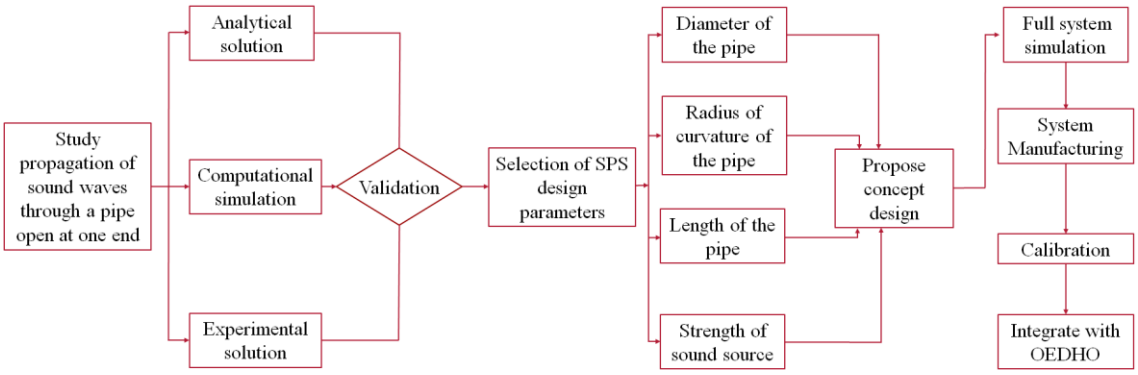

Fig. 4.1. Flow chart of the SPS development.

5. Analytical modeling: acoustics theory

Acoustic waves constitute a kind of pressure fluctuation that can exist in a compressible fluid. Apart from audible pressure fields of moderate intensity, there are also ultrasonic and infrasonic waves whose frequency lie beyond the limits of hearing, high-intensity waves that may produce a sensation of pain instead of sound, nonlinear waves of even higher intensities, and shock waves generated by explosions and supersonic aircrafts [Kinsler and Frey, 1986].

Inviscid fluids exhibit fewer constraints to deformations than solids. The restoring forces responsible for propagating a wave are the pressure changes that occur when the fluid is compressed or expanded. Individual elements of the fluid move back and forth in the direction of the forces, producing regions of compressions and rarefaction.

In order to describe the propagation of sound in any fluid medium, a single equation can be derived by correlating the acoustic pressure with adiabatic bulk modulus $\mathcal{B}$ as, linear continuity equation, and linear Euler's equation

$$P = \mathcal{B}s. \tag{5.1}$$

$$\rho_0 \frac{\partial s}{\partial t} + \nabla \cdot \bar{u} = 0. \tag{5.2}$$

$$\rho_0 \frac{\partial \bar{u}}{\partial t} = -\nabla p. \tag{5.3}$$

where, p is the acoustic pressure at (x, y, z), s is condensation at (x, y, z) , $\bar{u}$ is particle velocity of a fluid element, t is time, and ρ_0 is equilibrium density [Kinsler and Frey, 1986]. Result of combining and simplifying Eqs. 5.1, 5.2, and 5.3 yields, linear lossless wave equation,

$$\nabla^2 p - \frac{1}{C_s^2} \frac{\partial^2}{\partial t^2} p = 0. \tag{5.4}$$

5.1. Solution of three-dimensional homogenous wave equation

In order to synthesize the sound presentation system carrying acoustic stimulus through the pipe, sound waves propagation through a pipe with circular cross section is studied by solving the wave equation, Eq. 5.4, in cylindrical coordinates. Inputting boundary conditions into the generic solution of the wave equation would provide analytical analysis of the system behavior.

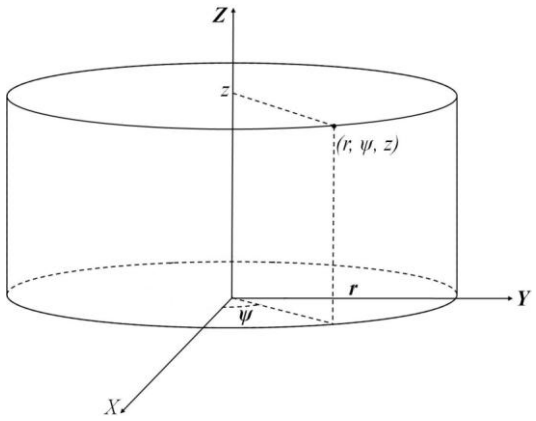

Fig. 5.1. The cylindrical coordinate system used in the analysis.

Consider three-dimensional, lossless, homogenous wave equation in the cylindrical coordinate system as shown in Figure 5.1,

$$\nabla^2\varphi(t,r) - \frac{1}{C^2}\frac{\partial^2}{\partial t^2}\varphi(t,r) = 0, \tag{5.5}$$

where ∇^2 is the Laplacian defined as

$$\nabla^2 = \frac{\partial^2}{\partial r^2} + \frac{1}{r}\frac{\partial}{\partial r} + \frac{1}{r^2}\frac{\partial^2}{\partial \psi^2} + \frac{\partial^2}{\partial Z^2}, \tag{5.6}$$

with $\varphi(t,r)$ being the velocity potential (m^2/s), and C_s is the speed of sound (m/s).

When speed of sound is constant, the fluid medium is referred to as a homogenous medium. The wave equation, Eq. 5.4 is considered to be homogenous equation as there is no forcing function associated with it.

Solution of the Eq. 5.4. is obtained by assuming that the velocity potential $\varphi(t,r)$ has a time-harmonic dependence,

$$\varphi(t,\boldsymbol{r}) = \varphi_f(\boldsymbol{r})e^{+i\omega t}, \tag{5.7}$$

where, the angular frequency $\omega = 2\pi f$, $\varphi_f(r)$ is spatial dependent part of the velocity potential, and f is frequency in Hz.

By substituting Eq. 5.7 into Eq. 5.5 the time independent lossless Helmholtz equation is obtained,

$$\nabla^2\varphi_f(\boldsymbol{r}) + k^2\varphi_f(\boldsymbol{r}) = 0. \tag{5.8}$$

where k is the wave number defined as,

$$k = \frac{2\pi f}{c_s}. \tag{5.9}$$

Solution of Eq. 5.8 can be obtained by the method of separation of variables. by setting,

$$\varphi_f(\boldsymbol{r}) = \varphi_f(r,\psi,z) = R(r)\Psi(\psi)Z(z). \tag{5.10}$$

by substituting Eq. 5.10 into Eq. 5.8 and simplifying, produces,

$$\frac{1}{R(r)}\frac{\partial^2}{\partial r^2}R(r) + \frac{1}{rR(r)}\frac{\partial}{\partial r}R(r) + \frac{1}{r^2\Psi(\psi)}\frac{\partial^2}{\partial \psi^2}\Psi(\psi) + k^2 = -\frac{1}{Z(z)^2}\frac{\partial^2}{\partial Z^2}Z(z). \tag{5.11}$$

Second ordered partial derivatives with respect to r,ψ,z are reduced to ordinary second-ordered derivatives since $R(r),\Psi(\psi), and\ Z(z)$ are dependent on only one variable, i.e., $r,\psi, and\ z$, respectively.

The first separation of variables is obtained by setting the right hand component of Eq. 5.11 to

$$-\frac{1}{Z(z)^2}\frac{\partial^2 Z(z)}{\partial Z^2} = k_z^2. \tag{5.12}$$

Equation 5.12 is a second–order homogenous ordinary differential equation with solution of the form

$$Z(z) = A_z e^{-ik_z Z} + B_z e^{+ik_z Z} \tag{5.13}$$

with Eq. 5.13, the direction of the travelling wave can be determined based on the value of k_z. If k_z is positive then, $A_z e^{-ik_z Z}$ represents plane wave travelling in positive *z* direction and $B_z e^{+ik_z Z}$ represents plane wave travelling in negative *z* direction.

To prove this, for first term on right hand-side of the Eq. 5.13, consider a function,

$$Z(t,z) = A_z e^{\left[-ik_z\left(z-\frac{2\pi f}{k_z}t\right)\right]} \tag{5.14}$$

Equation 5.14 shows that, as time t increases, the wave moves in positive *z*-direction. Similarly, second term on the right hand side of Eq. 5.14 represents a wave travelling in negative *z*-direction.

Since the left hand side of the equation 5.12 is equal to k_z^2, multiplying both sides of equation 5.11. by r^2, and substituting $k_r^2 = k^2 - k_Z^2$,

$$\frac{r^2}{R(r)}\frac{d^2}{dr^2}R(r) + \frac{r}{R(r)}\frac{d}{dr}R(r) + k_r^2 r^2 = -\frac{1}{\Psi(\psi)}\frac{d^2}{d\psi^2}\Psi(\psi). \tag{5.15}$$

A subsequent separation of variables is obtained by setting the right hand side of Eq. 5.15 to a constant with,

$$-\frac{1}{\Psi(\psi)}\frac{d^2}{d\psi^2}\Psi(\psi) = n^2. \tag{5.16}$$

On simplifying Eq. 5.16, its solution is obtained in the form of

$$\Psi(\psi) = A_\psi^{'} e^{-in\psi} + B_\psi^{'} e^{+in\psi}. \tag{5.17}$$

Substitution of Eq. 5.16 back into Eq. 5.15 yields the equation with only one variable *r*. Therefore, Eq. 5.11 can be written in terms of only one variable r by utilizing Eqs. 5.12 and 5.16 to yield

$$\frac{d^2}{dr^2}R(r) + \frac{1}{r}\frac{d}{dr}R(r) + \left(k_r^2 - \frac{n^2}{r^2}\right)R(r) = n^2. \tag{5.18}$$

Substituting $R(r) = g(k_r r)$, Eq. (5.18) becomes a *Bessel differential equation* with solution

$$R(r) = A_r J_n(k_r r) + B_r Y_n(k_r r). \tag{5.19}$$

Upon substituting Eqs. 5.19, 5.17, and 5.13 into Eq. 5.10, the general solution of the Helmholtz equation in cylindrical coordinates is,

$$\varphi_f(r,\psi,z) = [A_r J_n(k_r r) + B_r Y_n(k_r r)]\left[A_\psi \cos(n\psi) + B_\psi \sin(n\psi)\right] \times \left[A_z e^{-ik_z z} + B_z e^{+ik_z z}\right]. \tag{5.20}$$

$A_r, B_r, A_{\psi,} B_\psi, A_z, B_{z,}$ are all constants dependent on the boundary conditions, J_n and Y_n are Bessel functions of nth –order of the first and the second kind, respectively [McLachalan, 1961]. Equation 5.20 is the solution of the Helmholtz equation that relates the wave number *k* to the propagation vector components k_r and k_z

If the fluid medium occupies an angular sector $\psi_1 \leq \psi \leq \psi_2$ around the *z*-axis, which is less than 360^o, then the value of n is satisfied by conditions at the ends of angular sector $\psi = \psi_1$ and $\psi = \psi_2$ but, if the medium completely surrounds the *z*-axis then $\Psi(\psi)$ has a periodic value of 2π [Kinsler, and Frey A, 1986].

The general solution oh the homogenous Helmholtz equation has three independent terms. First term depending on the propagation of sound in radial direction, second term depending on the propagation on sound in angular direction, and the third term depending on the propagation of sound in axial direction.

6. Analytical solution of sound waves propagation through a pipe

Consider a pipe open at one end with the cross sectional area equal to (πa^2), where a is the radius of the pipe and it is l meters in length. The point sound source is located along the longitudinal axis of the cylinder and at the center of the closed face of the circular pipe.

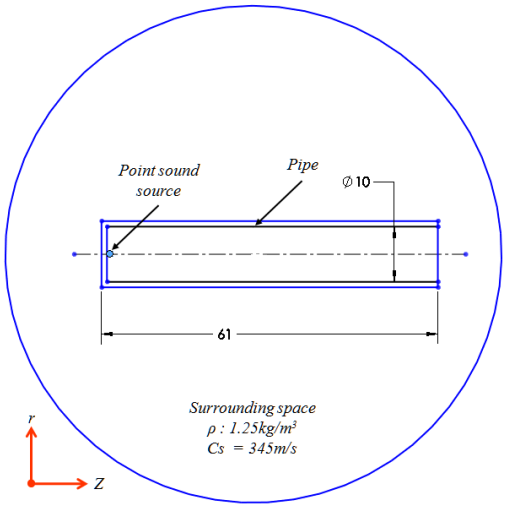

Fig. 6.1 Schematic of the test setup: pipe open at one end with a point sound source placed along the longitudinal axis and at the center of the closed surface,(ρ) Air density, (C_s) Speed of sound in air.

6.1. Assumptions

1. The acoustic medium is a frictionless, homogenous fluid.
2. The fluid medium is same inside and outside the pipe so there is no impedance mismatch.
3. The processes associated with the wave motion are isentropic.
4. The wave propagation remains wholly axial and directed along positive z.
5. The pipe walls are rigid and continuous; there are no losses due to viscosity or boundary layer formation.

6.2. Analytical solution of acoustic pressure distribution inside a pipe with circular cross section.

In this section we shall derive expressions for the velocity potential and the acoustic pressure inside a cylindrical cavity. Since we are interested in acoustic field inside the pipe at $r=0$, we shall modify solution of Helmholtz equation, Eq. 5.20 and take $B_r=0$ as the starting point. As the fluid completely surrounds the *z*-axis, values of n must be integers. Therefore Eq. 5.20 becomes

$$\varphi_f(r,\psi,z) = [J_n(k_r r)][A_n \cos(n\psi) + B_n \sin(n\psi)]\left[A_z e^{-ik_z z} + B_z e^{+ik_z z}\right], \quad (6.1)$$

where, $A_n = A_r A_\psi$, $B_n = A_r B_\psi$, and $k_r^2 + k_z^2 = k^2$.

The values of the unknown constants $A_n, B_n, A_z,$ and B_z are determined by satisfying boundary conditions, which are defined next.

Similar to Eq. 5.7, the time – harmonic acoustic fluid velocity vector is given by

$$\boldsymbol{u}(t,r) = \boldsymbol{u}_f(r)e^{+j\omega t} \quad (6.2)$$

where, $\boldsymbol{u}(r) = \nabla\varphi_f(\boldsymbol{r})$, and

$$\nabla = \frac{\partial}{\partial \mathrm{r}}\hat{r} + \frac{1}{r}\frac{\partial}{\partial \psi}\hat{\psi} + \frac{\partial}{\partial \mathrm{z}}\hat{z} \quad (6.3)$$

Therefore, the normal component of the acoustic fluid velocity vector is:

$$u_n(t,r) = \hat{n}\cdot\boldsymbol{u}(t,r) = u_n(t,r) = \hat{n}\cdot\boldsymbol{u}(t,r) = u_{f,n}(r)e^{+i\omega t}, \quad (6.4)$$

with $\hat{n}$ is a unit vector normal to the inside surface of the pipe. The direction of unit vector is in outward direction i.e., from the center of the pipe towards its wall.

First boundary condition:

The unit vector normal to the closed surface at $z = 0$ pointing towards the open end is

$$\hat{n} = -\hat{z}, \quad (6.5)$$

as the normal component of the acoustic fluid velocity vector must be equal to zero on the rigid walls at $z = 0$. Therefore, Eq. 6.4 simplifies to

$$u_{f,n}(r,\psi,z) = -\frac{\partial}{\partial \mathrm{z}}\varphi_f(r,\psi,z)\Big|_{z=0} = 0. \tag{6.6}$$

Second Boundary condition:

At $r = a$, the unit vector normal to the pipe surface and pointing in outward direction is

$$\hat{n} = \hat{r}, \tag{6.7}$$

as the normal component of velocity vector must be equal to zero at the rigid wall, Eq. 6.4 becomes

$$u_{f,n}(r,\psi,z) = \frac{\partial}{\partial \mathrm{r}}\varphi_f(r,\psi,z)\Big|_{r=a} = 0, \tag{6.8}$$

and

$$J_n^{'}(k_r a)[A_n \cos(n\psi) + B_n \sin(n\psi)]2A_z e^{-ik_z z} = 0. \tag{6.9}$$

Since the Eq. 6.9 must be true for all values of *r, ψ,* and *z*,

$$B_n = A_n. \tag{6.10}$$

In order to satisfy the boundary condition at $r = a$, the propagation vector component in the horizontal radial direction is only allowed certain discrete values rather than a continuum of values.

Now, substituting Eq. 6.10 into Eq. 6.1 yields

$$\varphi_{f,n,l}(r,\psi,z) = J_n\left(\alpha_{n,l}\frac{r}{a}\right)\left[A_{n,l}\cos(n\psi) + B_{n,l}\sin(n\psi)\right]2A_z e^{-ik_z z}, \tag{6.11}$$

where $A_{n,l} = 2A_n A_z$, and $B_{n,l} = 2B_n B_z$.

The complete time-harmonic normal-mode solution for the velocity potential is therefore

$$\varphi(t,r) = \sum_{n=0}^{\infty}\sum_{l=0}^{\infty}\varphi_{f,n,l}(r)e^{i\omega t}. \quad (6.12)$$

By substituting Eq. 6.11 into Eq. 6.12, it is obtained,

$$\varphi(t,r,\psi,z) = \sum_{n=0}^{\infty}\sum_{l=0}^{\infty} J_n\left(\alpha_{n,l}\frac{r}{a}\right)\left[A_{n,l}\cos(n\psi) + B_{n,l}\sin(n\psi)\right]2A_z e^{-ik_z z}e^{i\omega t}. \quad (6.13)$$

Therefore, Eq. 6.13 can be expressed in terms of time-harmonic acoustic pressure as

$$p_{n,l}(t,\boldsymbol{r}) = -i\omega\rho_0\varphi_{n,l}(t,r)\sum_{n=0}^{\infty}\sum_{l=0}^{\infty}\varphi_{f,n,l}(r)e^{i\omega t}. \quad (6.14)$$

Therefore, $p_{n,l}(t,\boldsymbol{r}) = -i\omega\rho_0$, (6.15)

which results in,

$$p(t,r,\psi,z) = -i2\omega\rho_0\sum_{n=0}^{\infty}\sum_{l=0}^{\infty} J_n\left(\alpha_{n,l}\frac{r}{a}\right)\left[A_{n,l}\cos(n\psi) + B_{n,l}\sin(n\psi)\right].e^{-ik_z z}e^{i\omega t}. \quad (6.16)$$

Now, the values of the constants $A_{n,l}$ and $B_{n,l}$ are determined by using two more boundary conditions for location of sound source.

Third boundary condition,

at $z = 0;\ p = P1$ (6.17)

P1: Pressure at the point where the sound source is located.

Since, we are interested in sound pressure distribution along the longitudinal axis of the waveguide with circular cross section, values of $r, \psi = 0$

Fourth boundary condition,

$$\text{at}, z = Z1;\ p = p0. \tag{6.18}$$

$p0$ is the atmospheric pressure; *Z1* is situated at very large distance from the source.

Substituting the boundary conditions into the Eq. 6.16, normalizing with respect to $p0$, and simplifying, acoustic pressure along the longitudinal axis of the pipe is,

$$P = \omega\rho_0 C_s \frac{\sin[k(L-z)]}{coskl} sin\omega t, \tag{6.19}$$

where, *L* is the length of the pipe and *z* is the location along the length of the pipe.

The propagation of sound waves in *z*-direction along the longitudinal axis of the pipe depends on the angular frequency of the sound source, ω, density of the medium ρ_0, speed of sound C_s in air, and acoustic wave number, k. Since the equation is solved only along the longitudinal axis of the pipe, there are no radial and angular components in Eq. 6.19.

6.3. Computational simulation

COMSOL-Multiphysics software is used to simulate the acoustic field in open space and the structural interaction with solid objects [COMSOL, 2008]. The modules used for the analysis are: 1. Acoustic module – Pressure acoustics – Time - harmonic analysis. 2. Acoustic module – solid - stress –strain – frequency response analysis. A detailed procedure to build the computational model is described in appendix A.

6.3.1. Model definition

The model demonstrates the propagation of acoustic field inside the pipe closed at one end, with geometric dimensions of a = 10 mm, l =61 mm, and t = 0.5 mm and the surrounding field in 3D space. An acoustic source is placed at the center of the closed end of the cylinder. The acoustic waves created by the acoustic source are reflected from the cylinder walls before exiting from the open end of the pipe in the surrounding space. Figure 6.2 illustrates the acrylic cylinder model fixed on the closed end with air as the fluid domain.

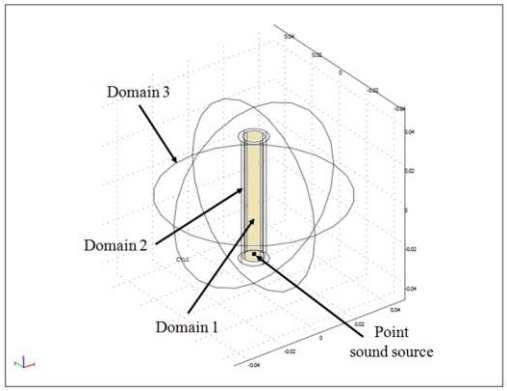

Fig. 6.2. Computational simulation setup:
domain 1: Air column inside the pipe;
domain 2: acrylic plastic pipe, 10mm in diameter,
61mm in length; domain 3: surrounding air.

6.3.2. Sub-domain settings

1. Air sub-domain (domain 1 and domain 3)

For harmonic sound waves the frequency-domain Helmholtz equation for sound pressure,

$$\nabla.\left[-\frac{1}{\rho_0}(\nabla p - q)\right] - \frac{\omega^2 p}{\rho_0 c_s^2} = 0, \tag{6.20}$$

with

$$p = p_0 e^{i\omega t}, (N/m^2). \tag{6.21}$$

The fluid properties applied to the air sub-domain are $\rho_0 = 1.25\ kg/m^3$, $C_s = 343\ m/s$

2. Solid sub-domain (domain 2)

The harmonic stresses and strains inside the solid pipe walls are defined by using the frequency response analysis in the 3D Solid, Stress-Strain application mode. The material properties of the pipe are: Young's modulus (E): 3.2GPa , Poisson's ratio (υ): 0.35, Density (ρ)*:* 1160 kg/m^3.

6.3.3. Boundary settings

6.3.3.1 Radiation boundary condition

Sub-domain 3 which depicts the surrounding space is assigned radiation boundary condition and spherical wave parameter. The radiation conditions allows an outgoing wave to leave the modeling domain with no or minimal reflections. There are three ways to specify the type of wave for radiation boundary condition [Bogey and Bailly, 2002],

1. Plane
2. Cylindrical
3. Spherical

The selection of the wave type is based on the geometry of the object. In present case, surrounding space is defined by a sphere and hence spherical wave type is selected.

6.3.3.2. Normal acceleration condition

The normal acceleration condition is used to couple the acoustic pressure wave to the solid pipe with boundary load F (force/unit area) assigned to the pipe,

$$F = -n_s(P), \tag{6.22}$$

n_s is the outward pointing unit normal vector directed from center of the pipe.

To couple the frequency response of the solid to the acoustics module, a boundary condition that specifies the normal acceleration equal to the solid structure is used,

$$-n_a\left[-\frac{1}{\rho_0}(\nabla p)\right] = a_n, \tag{6.23}$$

with n_a is the outward pointing unit normal vector directed from inside the acoustic domain.

6.3.4. Point source settings

A point source is a single identifiable localized source of sound. A point has negligible dimension, distinguishing it from other source geometries. Sources are modeled as point sources because in mathematical and computational modeling these sources can be approximated as a mathematical point to simplify the analysis.

In present case, the sound waves are generated by a point sound source with power *P* =0.2 W is specified as the strength of the source.

6.3.5. Mesh generation parameters

For solving the practical problems using finite element analysis, the geometry under consideration is divided in large number of small elements, typically triangles or quadrilaterals in two dimensions and tetrahedral or hexahedral in three dimensions. Two consecutive elements in a mesh intersect only at shared edges and vertices.

(a) (b)

Fig. 6.3. Mesh element type: (a) tetrahedral element (b) hexahedral element.

In present models, tetrahedral elements are used. The size of the element is defined by assigning minimum number of elements required per wave number.

Frequency range in this problem is 25 Hz to 8 KHz therefore,

Wave number $k = 2\pi f / c_s$. (6.23)

Based on the wave number for the maximum frequency in the frequency range, tetrahedral geometry is defined by taking number of elements per wave number equal to 2, 3 ,5, 8 and 10, Fig. 6.4. Then, the convergence of the solution based on different mesh sizes is plotted in terms of percentage error, as shown in Fig. 6.5.

Maximum element size = Wave number (k) × No. of elements (6.24)

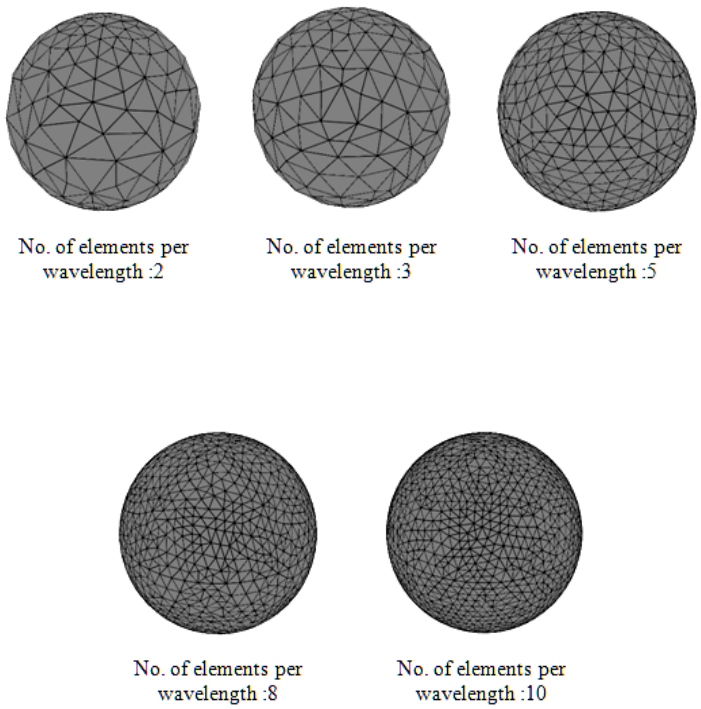

Fig. 6.4. Variation in mesh size by changing number of elements.

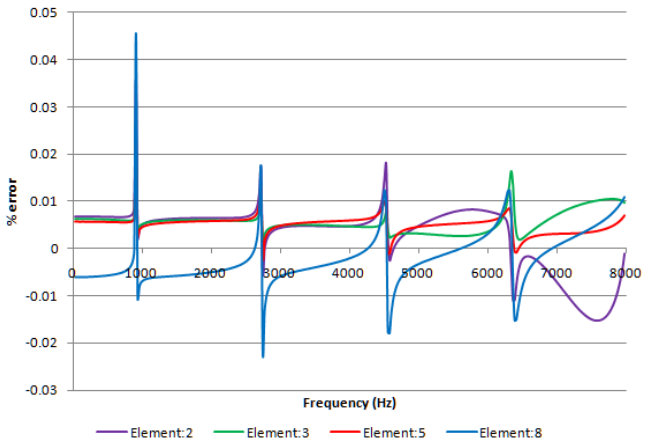

Fig. 6.5. Solution convergence plot for different mesh sizes.

To determine the optimum mesh size for all the computational simulations, the computational model is ran by selecting different number of elements for every wave number. COMSOL Multiphysics recommended maximum 10 elements per wavelength for most accurate solution; hence taking number of elements equal to 10 as the reference, the percentage error in all the simulations is calculated,

$$\%error = \frac{SPL_{(ele.:2,3,5,8)} - SPL_{ele:10}}{SPL_{ele:10}}. \tag{6.25}$$

The plot of frequency versus percentage error clearly indicates that simulation with 8 elements per wave number yields the most accurate computational solution, because for element 8 error plot is comparatively symmetrical across the frequency range as compared to other element sizes.

6.3.6. Solver specifications

Time-harmonic acoustics can be solved either with the stationary solver for a single frequency or with the parametric solver when a frequency range is specified. The frequency parameter is initially defined in the application scalar variables.

In the solver dialogue box, name of the parameter, initial value, final value and step size are entered. Next, type of linear system solver is selected.

In present case, frequency is the parameter, 'Freq' is the parameter name entered into application scalar variables. The range is defined with initial value as 24.5 Hz, final value as 8000 Hz., and step as 24.5 Hz.

Direct (SPOOLES) is the linear system solver used for this analysis [Li, 2002]. SPOOLES is a library for solving sparse real and complex linear systems of equations. A typical sparse solver consists of four distinct steps as opposed to two in the dense case:

1. An ordering step that reorders the rows and columns such that the factors suffer little fill, or that the matrix has special structure such as block triangular form.
2. An analysis step or symbolic factorization that determines the nonzero structures of the factors and creates suitable data structures for the factors.
3. Numerical factorization that computes the L and U factors.
4. A solve step that performs forward and back substitution using the factors.

6.3.7. Effect of change of domain size

Before proceeding with computational simulations for the synthesis of the sound presentation system (SPS), it is important to investigate if the surrounding domain has any effect on the computational simulation as shown in Fig. 6.6. To investigate these effects, the radius of spherical surrounding domain is changed from 40 to 60 mm with a step of 5 mm. and the comparison is plotted. Results shown in Fig. 6.7 show that there are minimum effects on the accuracy of the solution due to domain size.

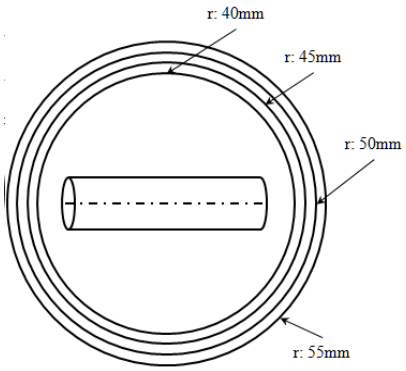

Fig. 6.6. Domain size variation.

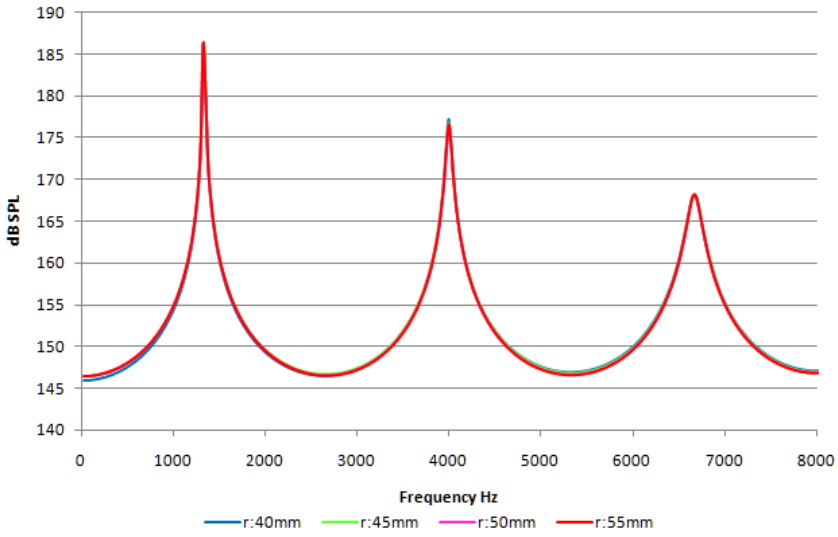

Fig. 6.7. Comparison plot of frequency response at different domain size.

6.4. Experimental investigations

An experimental study on the propagation of sound waves through a pipe closed at one end is carried out. The geometric dimensions of the acrylic pipe samples are a = 10 mm, l =60 mm, and t = 0.5 mm. An approximate point sound source is located at the center of the closed end of the pipe. Aim of this experiment is to measure the sound pressure level (SPL) distribution at different locations along the longitudinal axis of the pipe.

6.4.1. Test setup

Pipe under the study is mounted on a linear stage with a speaker at its closed end inside a sound proof chamber at the MEEI. Another linear stage is used to mount the microphone with a probe tube attached to it. Movement of microphone with respect to the longitudinal axis of the pipe allows us to probe the SPL at various locations. Experimental setup is shown in Fig. 6. 8

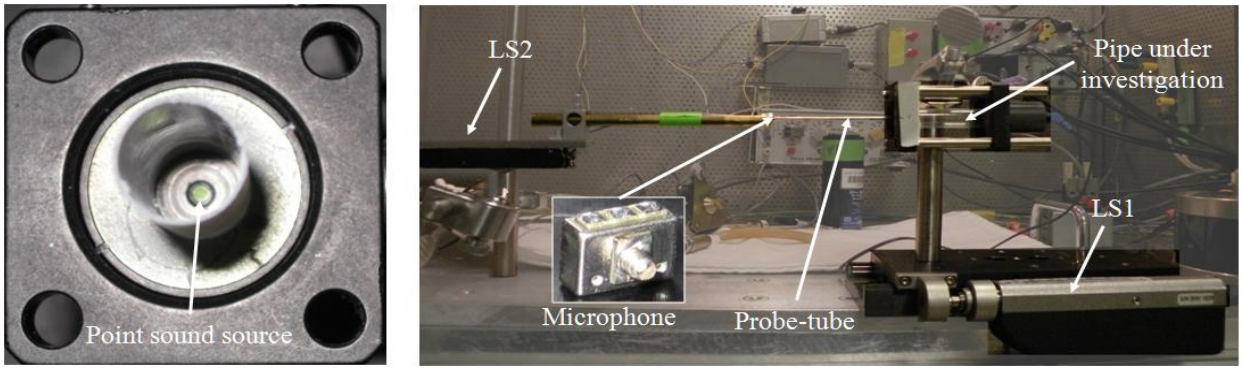

Fig. 6.8. Experimental setup: LS1: Linear stage 1, LS2: Linear stage 2.

6.4.2. System calibration

To measure the SPL inside the pipe, we calibrated the instrumentation used for performing this experiment. All the calibration process is done by recording frequency response of the

individual element in the experimental setup with the help of specially designed software developed at MEEI, see Fig. 6.9

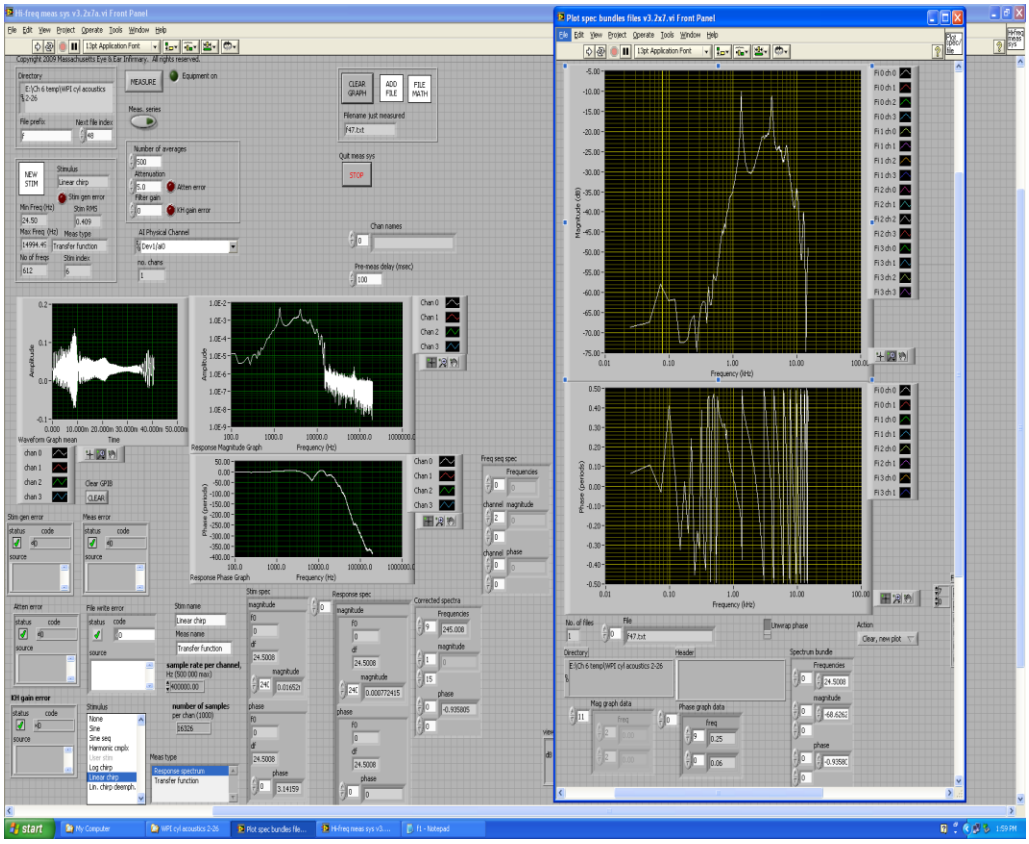

Fig. 6.9. Computer interface for SPL measurement.

Initially, the probe tube microphone used in the experiment is calibrated with a reference microphone which has a flat frequency response from 2 kHz to 100 kHz [Egolf, 1977]. To calibrate the probe- tube microphone, we inserted the probe tube into the side of the brass coupler attached to the reference microphone, by doing this we ensured that the probe tube tip was in the vicinity of the sound field around the reference microphone. Next, we measure the frequency response of the instrumentation used between the microphone, speaker and the computer interface. The instrumentation used for this experiment consists of analog to digital and digital to analog boards, reconstruction filter, the attenuator, and the power amplifier.

6.4.3. Experimental procedure

To measure the sound pressure level (SPL) along the length of the pipe, the probe tube was initially aligned along the longitudinal axis of the pipe and the tip of the probe tube is aligned perpendicular to the open face of the pipe. The reading on both the linear stages is noted, this reading served as origin position for all the readings. Subsequently, the probe-tube microphone was moved along the length of the tube with the help of linear stages

At the computer interface, the frequency range and frequency step was specified. Then, number of averages for the frequency range was selected and finally the attenuation level is determined by taking several rough measurements.

Next, the experimental tests were performed at different locations inside the tube and 10mm away from the open face of the tube. These tests were carried out along the center line of the pipe and also along the walls of the pipe, as illustrated in Fig. 6.10. the magnitude and phase of the microphone voltage measured with the probe tip at different locations and frequencies was saved using the computer interface.

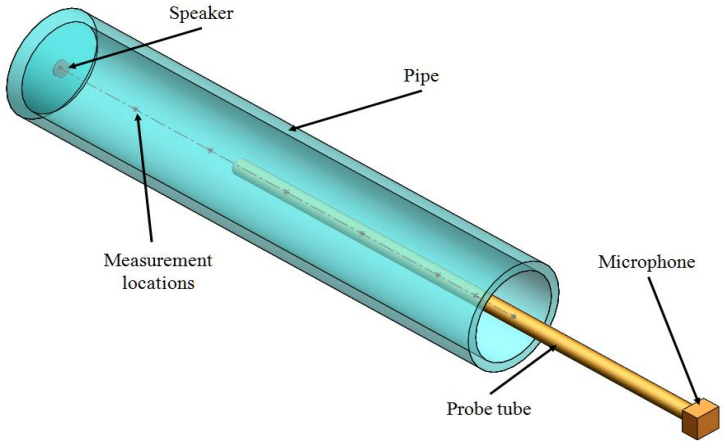

Fig. 6.10. Schematic of experimental setup realized to measure acoustic pressure along longitudinal axis of pipe.

6.4.4. Post processing of experimental readings

In order to plot the comparison of experimental, analytical and computational solutions, we needed correct for the, frequency response of the probe-tube microphone, amplifiers, filters, analog to digital and digital to analog boards. The first part of this correction was to normalize the measurements by a measurement at some control location. Method of normalization using ratios is often used to eliminate system related frequency-dependences from the experimental readings [Ravicz et al., 2007].

Method of normalization using ratios

The noise from the experimental readings is eliminated by initially normalizing the SPL recorded throughout the frequency range with respect to a particular frequency. This process is carried out for the frequency response recorded at a reference location (FR_{ref}) and also for the frequency response recorded at a location (FR_{exp}) under experimentation. Next, normalized frequency response FR_{ref} is divided by the FR_{exp}.

Step1: Normalization by a particular frequency (Present case: 500Hz),

$$step\ 1 = \frac{SPL_{(freq\_range)}}{SPL_{(freq\_ref)}} \tag{6.26}$$

Step2: Ratio of normalized frequency response at a location under experimentation to the normalized frequency response of the reference location.

$$step\ 2 = \frac{FR_{exp}}{FR_{ref}} \tag{6.27}$$

Step 3: Plot the SPL and for entire frequency range and compare with analytical and computational solution.

In order to plot the SPL distribution on same scale, similar procedure is carried out on analytical and computational results.

6.4.5. Results and comparison

The comparison plots of the analytical solution, computational simulations, and experimental results are plotted at four different locations along the center line of the pipe. Figures 6.11 to 6.14 show comparisons of solutions which indicate reasonable agreement.

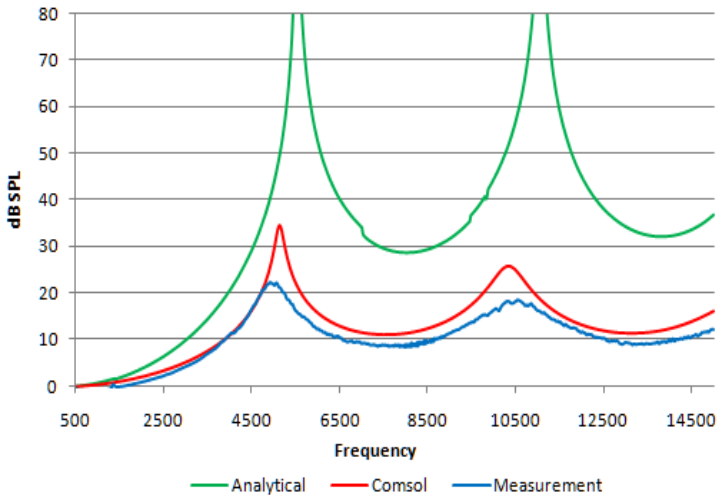

Fig. 6.11. Comparison plot of frequency response at a point 30mm away from the sound source.

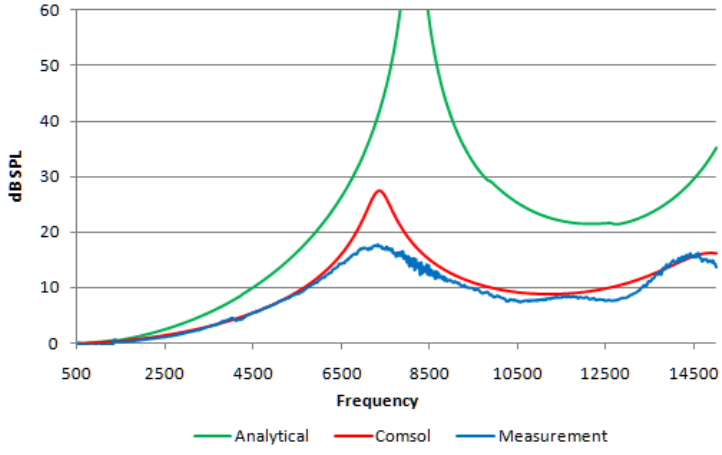

Fig. 6.12. Comparison plot of frequency response at a point 40mm away from the sound source.

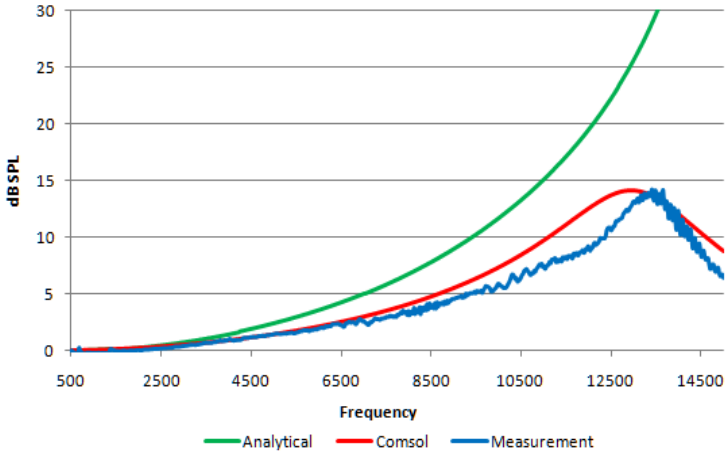

Fig. 6.13. Comparison plot of frequency response at a point 50mm away from the sound source.

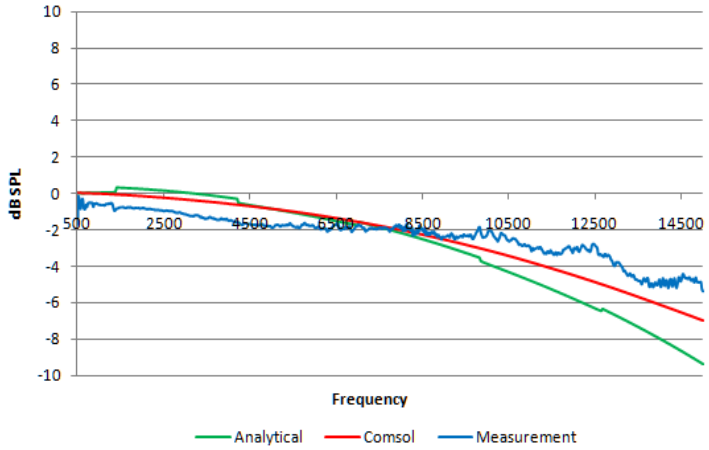

Fig. 6.14. Comparison plot of frequency response at a point 60mm away from the sound source.

The comparison plots show close match of frequency response between experimental readings and computational simulations. However, analytical solution shows noticeable differences. The probable reasons for the difference between the analytical solution with respect to experimental and computational solution include,

1. The analytical solution does not include damping from the pipe and effects of boundary layer formation.

2. The analytical solution is solved for far field, hence noticeable differences are expected in near field region. Same trend can be seen in the normalize plots, which show close match between experimental, computational and analytical solution as the distance between the source and the point under consideration increases.
3. The effect of end correction is also not taken into account for analytical solution, which also causes deviation in the analytical solution.

7. Synthesis of Sound Presentation System (SPS_V1)

To measure the displacements of the tympanic membrane using the OEHO system, a stimulus with known frequency and amplitude must be provided. This can be achieved with the help of an acoustic system. An integrated version of the acoustic system and the OEHO system will provide the complete package to diagnose the tympanic membrane. Synthesis of such a system is presented in further sections.

7.1. Initial design objectives and constraints

To design the system, initially design parameters are identified and then every parameter is synthesized individually.

The design parameters:

1. The dimensional constraints on the system design are based on the size and shape of the ear canal. A human ear canal has a curved profile with an approximate depth of 30 mm. The diameter of the TM is about 8-10 mm.
2. The system should be capable of producing 90-110 dB of sound pressure at 30 mm distance from the exit point of the SPS system.
3. The design of the SPS should not hinder the optical path of the OEHO system.
4. The SPS must be capable of interfacing with the standard medical speculums used for the ear examinations.
5. A special fixture is necessary in order to damp any vibrations produced from the speaker and the SPS body.
6. Based on the configurations of the OEHO systems, the design should be made compatible with all packaged versions.

7. The SPS should also be able to house a microphone to record the sound pressure at the tympanic membrane.
8. The system should not have any sharp edges as it will be in direct contact with the ear and sharp edges could cause injuries.

7.2. Effect of variation in pipe diameter on SPL

The first parameter investigated in the synthesis of SPS is the diameter of the pipe carrying acoustic stimulus. Three different diameters ranging from 3.8 mm to 10 mm are selected based on geometrical constraints with respect to design of the OEHO system.

The robust method developed and validated for the simulation of acoustic signal is utilized. Pipes of diameter 3.8 mm, 6 mm, and 10 mm each 60 mm in length are simulated inside free space sphere of 90 mm diameter. The simulation is carried out in the frequency range of 25 Hz to 8 kHz. [Hulli et al., 2007], and representative results are shown in Fig. 7.1. In addition, comparisons of frequency versus sound pressure level are plotted at a distance of 5mm from the open face of the pipe are shown in Fig. 7.2.

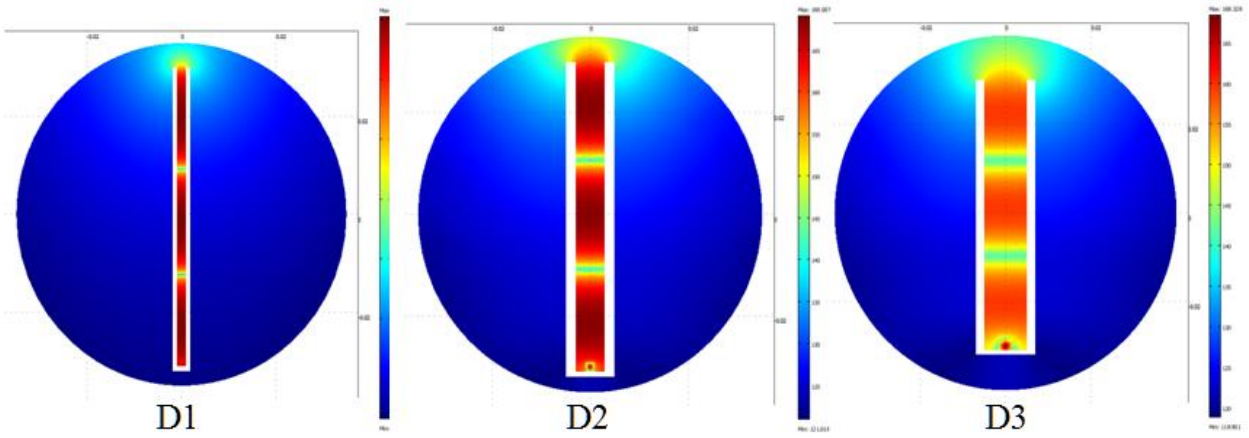

Fig. 7.1. Slice plot of computational simulations of SPL at 8 kHz;
diameter of the pipe: D1 = 3.8 mm, D2 =6 mm, D3 = 10 mm.

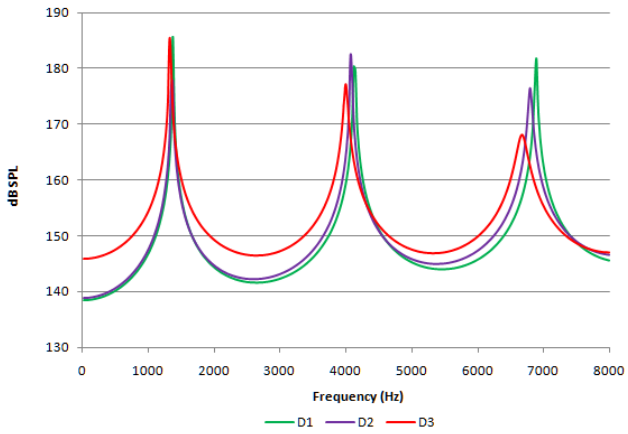

Fig. 7.2. Sound pressure distribution at 5mm distance from open face of the pipe; D1 = 3.8 mm, D2 =6 mm, D3 = 10 mm.

7.3. Effect of variation of pipe curvature on SPL

To account for the space constraints and adaptability with the OEHO system, it is important to understand the effect on SPL due to introduction of pipe curvature. The range of curvature to be introduced to the pipes is selected from the space constraint available around the OEHO system. Three pipe curvatures of radius 50 mm, 75 mm, and 100 mm are selected and analyzed using simulation procedure developed in preceding sections. Figures 7.3 and 7.4 show representative results.

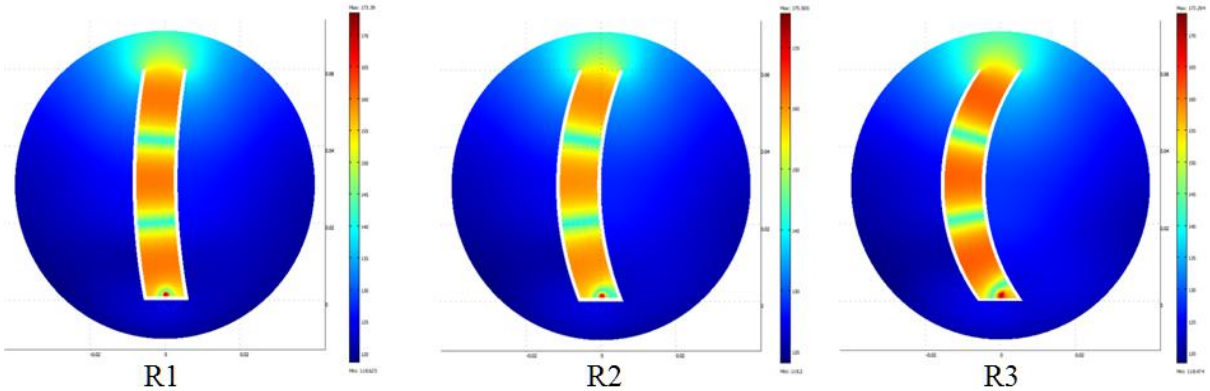

Fig. 7.3. Slice plot of computational simulations of SPL at 8 kHz; pipe curvature: R1= 100 mm, R2 = 75 mm, R3 = 50 mm.

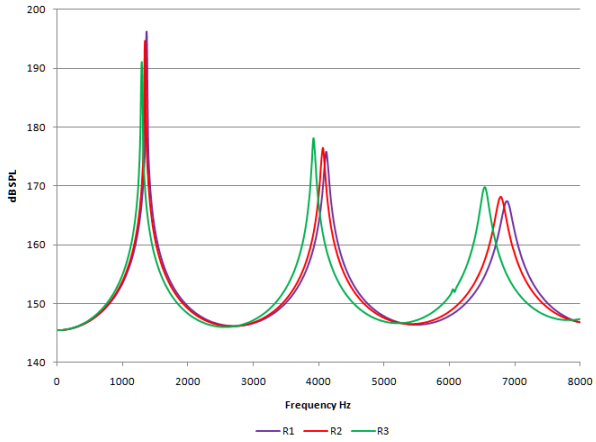

Fig. 7.4. Sound pressure distribution at 5mm distance from open face of the pipe; R1 = 100 mm, R2 = 75 mm, R3 = 50 mm.

7.4. Effect of variation of change in length on SPL

Final geometrical variation performed in order to select most efficient pipe combination is to change the length of the pipe carrying acoustic stimulus. It is important to locate the speaker away from the OEHO system in order to avoid effect of speaker vibrations on recording nanometer scale displacements on the TM. Knowledge gathered by varying the length of the pipes would help to realize possible location of the speaker in the system. Hence, sound pressure distribution with pipe lengths of 30 mm, 60 mm, and 90 mm are simulated. Figures 7.5 and 7.6 show representative results.

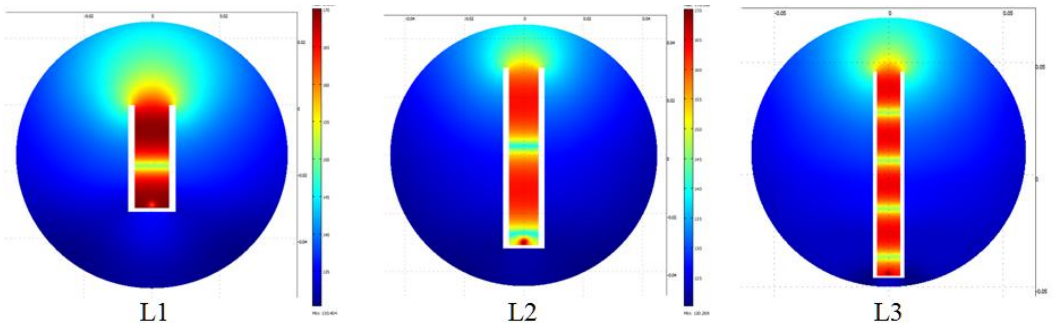

Fig. 7.5. Slice plot of computational simulations of SPL at 8 kHz; Length of pipe: L1= 30 mm, L2 = 60 mm, L3 = 90 mm.

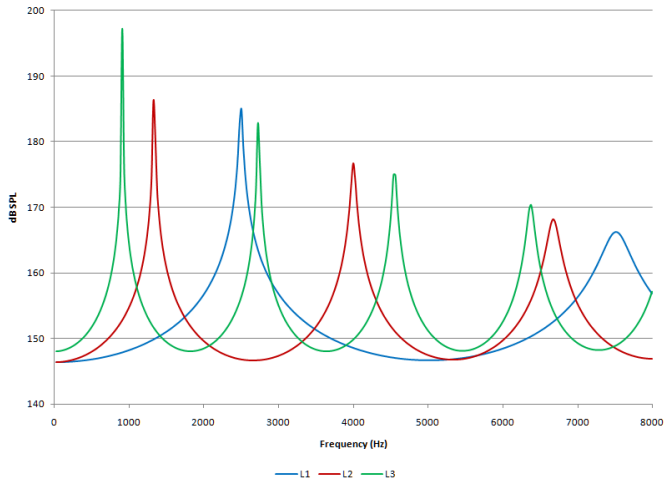

Fig. 7.6. Sound pressure distribution at 5 mm distance from open face of the pipe; L1 = 30 mm, L2 =60 mm, L3 = 90 mm.

7.5. Effect of variation in power of the point sound source on SPL

In addition to geometrical variations, it is important to realize effect of power of the sound source on the SPL. This is accomplished by simulating the sound waves propagation through a pipe 10 mm in diameter and 60 mm in length using three different power sources of 0.4 W, 0.6 W, and 0.8 W. The simulations would provide significant guidelines to select appropriate speaker for SPS design. Figures 7.7 and 7.8 show representative results.

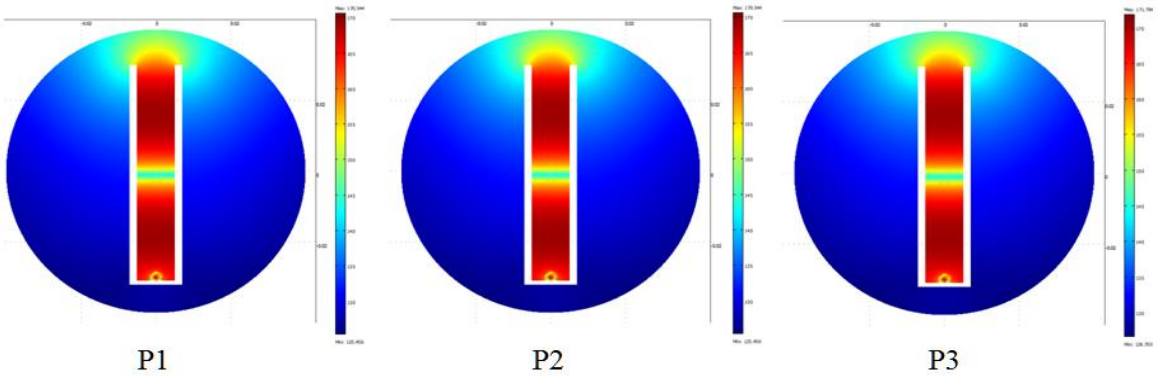

Fig. 7.7. Slice plot of computational simulations of SPL at 8 kHz; Length of pipe: P1 = 0.4 W, P2 = 0.6 W, P3 = 0.8 W.

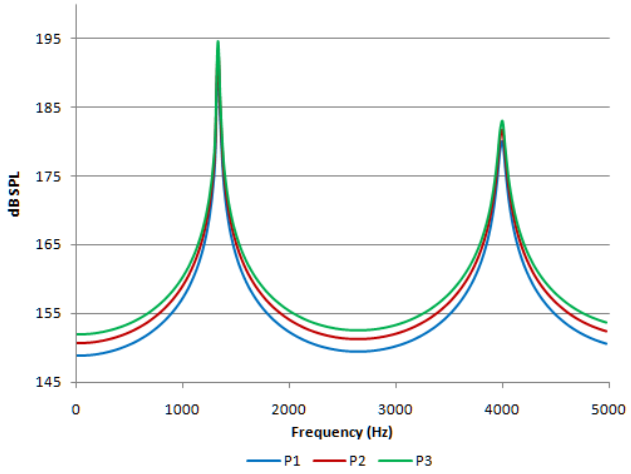

Fig. 7.8. Sound pressure distribution at 5 mm distance from open face of the pipe; P1 = 0.4 W, P2 = 0.6 W, P3 = 0.8 W.

7.6. Analysis of results from parametric investigation

The knowledge gained from the parametric investigation provided the guidelines to select the configuration of the SPS.

1. Pipe with diameter D3 produces higher sound pressure levels (6-8 dB) than diameter D1 and D2. However, the end correction affects the sound pressure levels at higher frequencies. Sound pressure level for the pipe with diameters D1 and D2 show differences in the range of 2-3dB. The effect of end correction appears to be highest with diameter D3, and lowest with diameter D1. Based on these results and to accomplish the miniature dimensions of the SPS system, diameter D1 is selected.
2. Introduction of the curvature to the pipe shows negligible change in the sound pressure levels. The position of the peaks in the frequency response plot appear to be shifted left as the radius of curvature is increased. Observing the same sound pressure levels for different radius of curvatures provides freedom to select the necessary curvature configuration in the design of the SPS.

3. Changing the length of the pipe provides important insight for selecting the dimensions of the system to be fitted on the otoscope head. In the same frequency range, the number of nodes increased from 2 for pipe with length L1 to 4 for pipe with length L3. Pipe with length L3 causes a 3-5dB rise in the pressure levels as compared to the pipe with length L1 or L2. As the length of the pipe determines the location of the sound source with respect to the otoscope head in the design of the SPS, pipe of length between 30 to 60mm is recommended.
4. Variation in the power of the point sound source confirmed the predictions that increase in the power will increase the sound pressure levels.

7.7. Concept design of the SPS_V1

A concept design of the SPS is proposed by considering the design objectives and parametric investigation. The concept is based on the design of a Welch Allyn otoscope head [Welch Allyn, 2010]. In the otoscope head, the laser light is impinged perpendicularly from a ring of the optic fiber bundle leaving the path open for the backscattered laser light to reach the camera. Similarly, the sound could be impinged symmetrically with the help of two pipes, derived from the same sound source located further back on the otoscope head. The microphone could be embedded in the body of the SPS and sound pressure at the tympanic membrane can be measured with the help of a probe tube. Figure 7.9 shows synthesized design of the SPS based on parametric models that were developed and described in pervious Sections.

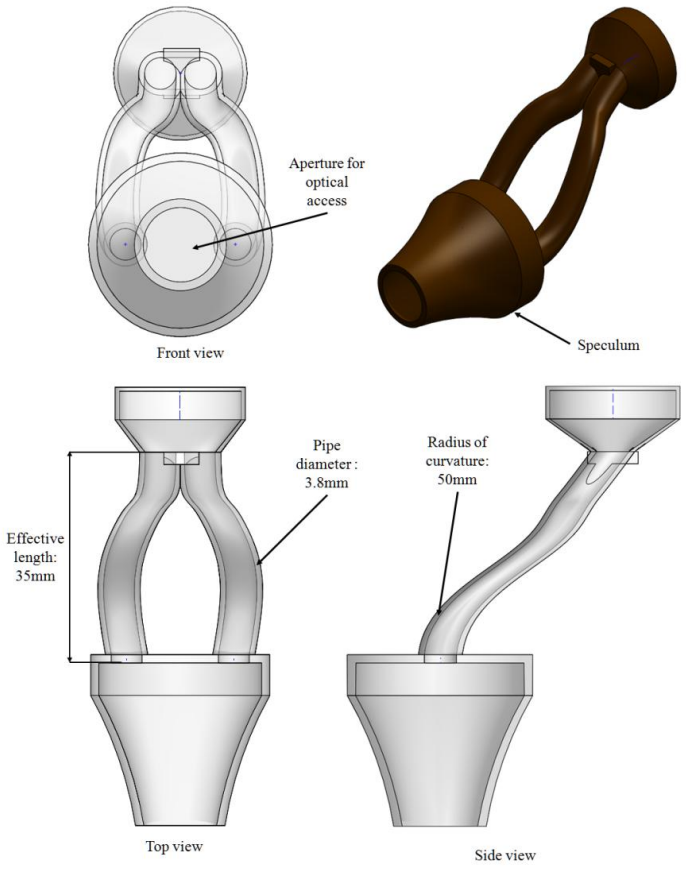

Fig. 7.9. Synthesized design of the SPS_V1 design is based on parametric models described in pervious Sections.

7.7.1. Design requirements

The outer diameter of the otoscope head tip is taken as a reference position for the entire design. The main advantage gained by selecting this reference position is that any hindrance in the optical path is theoretically eliminated. That satisfies one of the objectives of the system design.

The pipes carrying acoustic signal are 3.8 mm in diameter. As parametric investigation revealed no effects on the sound pressure level due pipe curvature, radius of curvature of 50 mm is modeled at two locations along the length of the pipe. This feature allows us to fit the SPS

around the otoscope head. The equivalent length of each pipe carrying the acoustic stimulus is 35 mm. This length satisfies the length constraint set by parametric investigation.

7.7.2. System requirements

After establishing the fundamental design of the system, the pipes, microphone and speaker are positioned in a casing. The SPS_V1 casing is made to fit around the otoscope body and concentrically align the aperture, for the optical access on the SPS, with the tip of the otoscope head. The system is designed to work with any speaker which is less than 15mm in diameter. Also, a special fixture is designed to split a sound signal symmetrically; as an input to the pipes carrying acoustic stimulus, shown in Fig. 7.10.

The microphone installed in this version of SPS is a Knowles microphone, $3\ mm \times 4\ mm$ in dimension and has smooth frequency response from 50 Hz to 20 kHz. The small dimension of the microphone facilitated its location directly at the tip of the SPS which allows measuring the sound pressure at the tympanic membrane. This in turn excluded the use of a probe tube from the design. A conduit is provided in the SPS casing to carry the electrical connections of the microphone and speakers.

Another objective is achieved by introducing interfacing fixture to the SPS_V1 body which allows interfacing with both of the packaged versions of the otoscope head that WPI/ CHSLT labs and MEEI have developed, see Fig. 7.11.

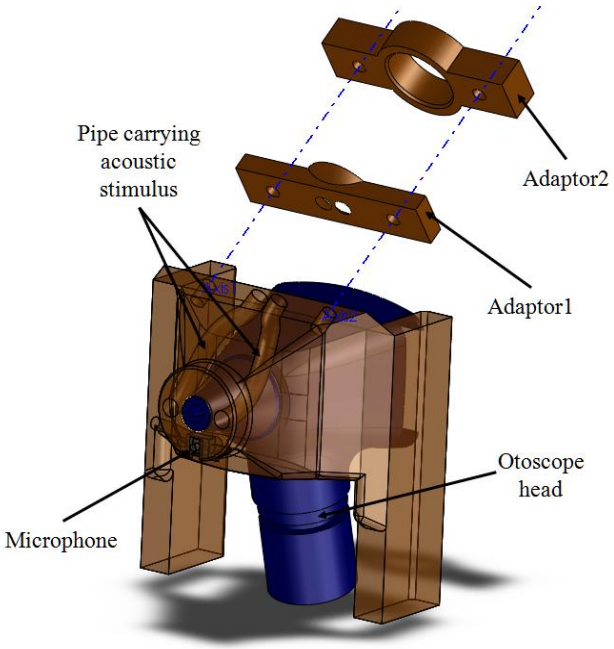

Fig. 7.10. CAD model of the proposed configuration of the SPS_V1; adaptor 1: symmetrically splits the sound signal from the speaker, adaptor 2: fixture to hold speaker up to 15 mm diameter.

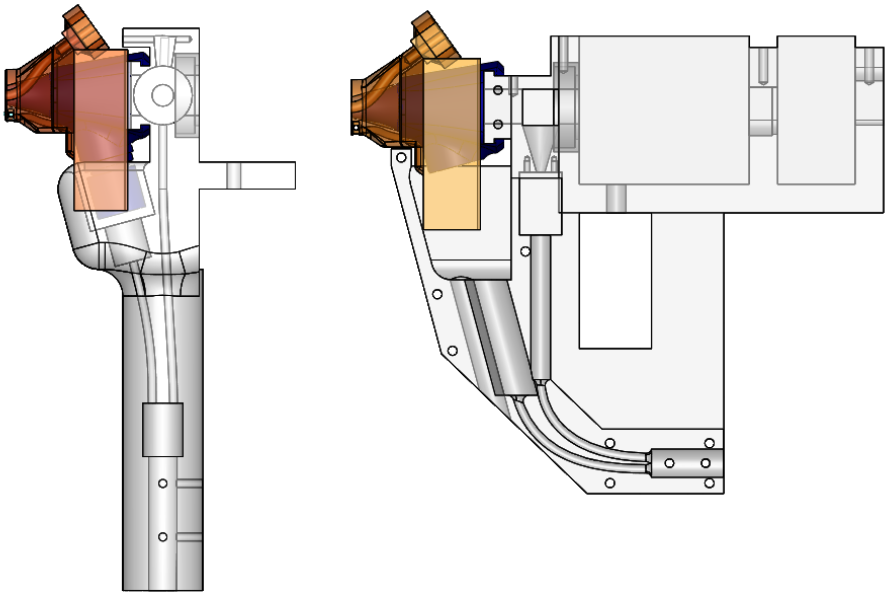

Fig. 7.11. SPS_V1 interfaced with two packaged versions of the OH system that WPI/CHSLT labs and MEEI has developed.

7.7.3. Computational simulation of SPS_V1

Parametric investigation provided the guidelines for selecting the optimum performance combination of the SPS. After fulfilling the design requirements, FEA is carried out on the entire concept design.

7.7.4. Model definition

In order to simulate entire SPS_V1, the pressure acoustics module and solid stress-strain modules are used from the COMSOL-Multiphysics software. To import the CAD model into FEA domain, all the dress-up features and components apart from pipe, speaker fixture, and speculum are removed to minimize the computer memory requirement and reduce the computation time. The SPS_V1 model is further simplified by assuming a point sound source instead of a speaker. Similar to previous finite element models, the SPS_V1 model is also contained inside a domain which defines the surrounding space with air as the propagation medium shown in Fig. 7.12. Domain 1 is a vibrating air column inside the pipes carrying acoustic stimulus. The speculum is also modeled in domain 1 with air as the propagation medium.

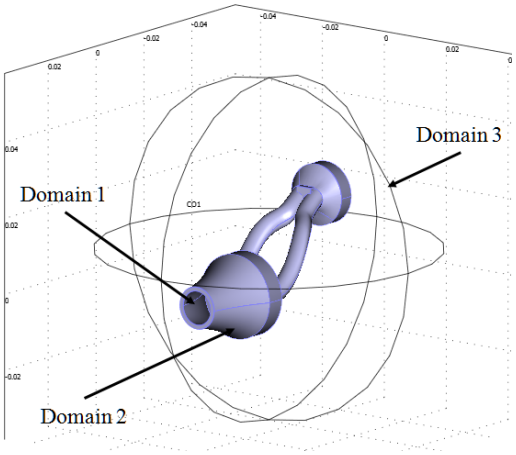

Fig. 7.12. FEA model of the synthesized SPS_V1 design.

Domain 2 is SPS_V1 itself. Inner walls of SPS_V1 are assigned a normal acceleration condition to enable fluid to structure interaction. Due to substantial wall thickness of the concept SPS_V1 design, the vibrations of the pipes due to propagation of sound waves through them are negligible. To take this effect into account, the outer walls of domain 2 are fixed. Domain 3 is also given a radiation boundary condition with spherical wave parameter to eliminate the reflected waves back into the domain.

7.7.5. Mesh generation

Figure.7.13 shows the meshed FEA model of the SPS_V1. The mesh parameters are selected based on the convergence plot in Fig. 6.5. To reduce the computation time and memory requirement without compromising the accuracy of the solution, a coarse mesh with 3 elements per wave number are assigned to domain 3, whereas the complexity of the SPS_V1 design requires fine mesh size (8 elements per wave number) to generate a sustainable mesh for the entire available frequency range between 25 Hz to 8 kHz.

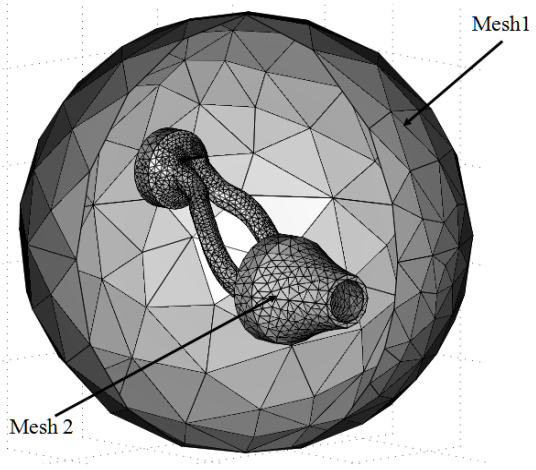

Fig. 7.13. The SPS_V1 mesh: Mesh1: coarse mesh with 3 elements per wavelength; Mesh 2: fine mesh with 8 elements per wavelength.

7.7.6. Solver specifications and post-processing

A parametric solver with frequency as the parameter is used to simulate the behavior of the SPS_V1. The frequency is varied in the range of 25 Hz to 8 kHz with 25 Hz frequency increments. Figures 7.14 and 7.15 show representative results.

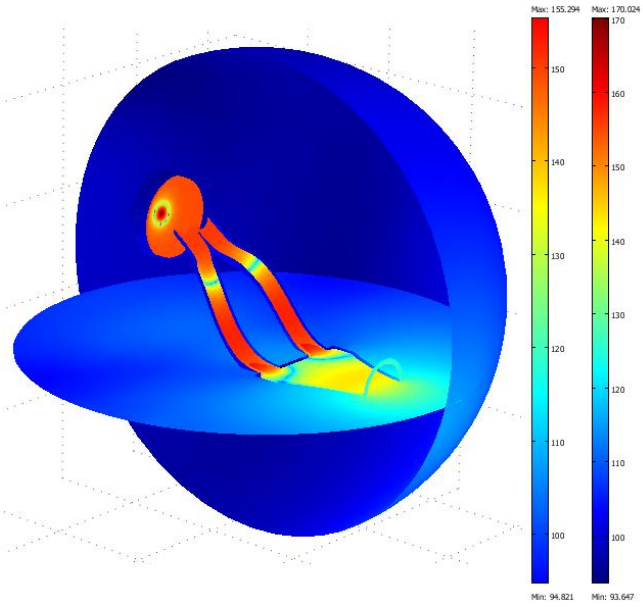

Fig. 7.14. Slice plot of the SPS_V1 simulation with suppressed boundaries showing sound pressure level inside the system and in the surrounding space at 8 kHz.

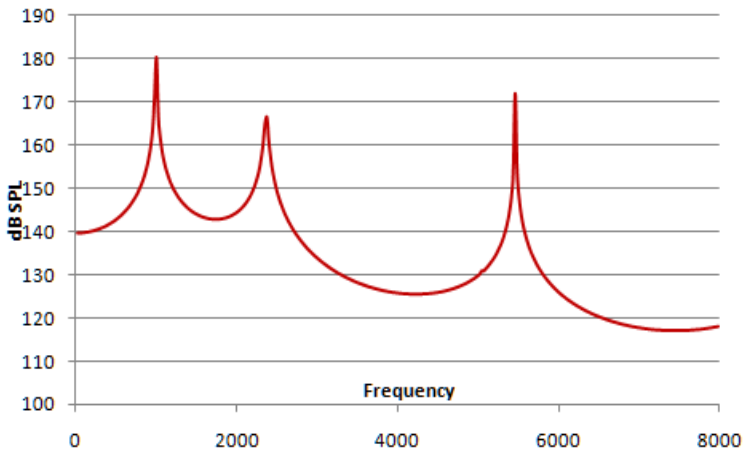

Fig. 7.15. Frequency response of the SPS_V1 at 5 mm distance from speculum end tip.

7.8. Fabrication of the SPS_V1

After computational modeling and analysis, the SPS_V1 was manufactured using stereo-lithography available at WPI and MEEI. Acura-60 is the material used for this process. The material properties of the Acura- 60 include, density ρ = 1210kg/m3, modulus of elasticity E = 2.6-3.1GPA. The fabricated model with tolerance of 10 microns is shown in Fig. 7.16 used.

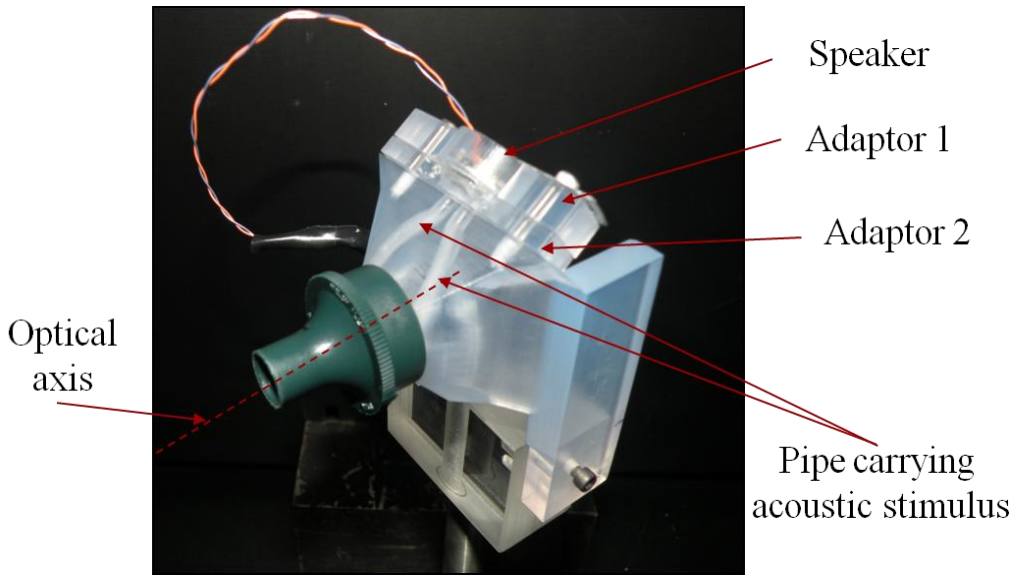

Fig. 7.16. Fabricated SPS_V1.

The positioning attachments and speaker interface is drilled into the fabricated prototype and the fixture for the speaker and the body of the SPS_V1 is sealed with hot glue to avoid any sound leakage. The speaker is constrained with a spring plate and the speaker and microphone wiring is channelized with an extra feature provided on the SPS_V1 body.

8. Experimental testing and validation of the SPS_V1

To determine performance characteristics and optimum setup combination it is required to carry out extensive testing of SPS_V1. SPS_V1 is put under battery of tests.

a. Effect on OH performance due to integration of SPS_V1

b. Effect of environmental noise on the operation of SPS_V1

c. SPS_V1 Performance optimization by varying set up combinations such as speakers, number of pipes carrying acoustic signal, distance from the TM, etc.

8.1. Effect on OEHO performance due to integration of SPS_V1

Shown in Fig. 8.1 a cantilever beam of known dimensions is tested with integrated setup of the SPS_V1 and OH. Fields of view, depth of field, SPS_V1 vibration effects, are the parameters investigated. The beam is made up of copper and is 5.7 mm in length, 3.5 mm in width, and 0.025 mm in thickness and is excited with the acoustic stimulus from the SPS_V1. First four bending modes of vibration of the beam are recorded using the OEHO system and frequency at every bending mode is compared with natural modes of vibration of the beam computed analytically and computationally.

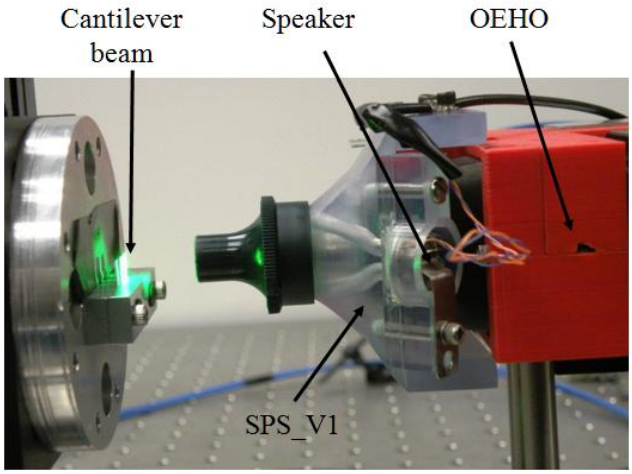

Fig.8.1. SPS_V1 integrated onto optical head OH.

The cantilever beam is being held with the help of a clamp to ensure fixed boundary conditions. The beam is coated with holographic dust and then measured with the help of an optical microscope to obtain its accurate dimensions for analytical and computational solutions. Next, the beam is aligned with the optical path of the OEHO system to perform the tests. The acoustic stimulus is controlled with the help of a function generator.

The analytical solution is computed by calculating the natural frequencies of vibration of the cantilever beam by:

$$\omega_n = \frac{r_n}{L^2}\sqrt{\frac{EI}{\rho A}} \tag{8.1}$$

where, E: Young's modulus; I: Moment of inertia of the beam section; ρ: Density; L: Length of the beam; A: Cross section; *r:* Constant.

Computational simulation of the cantilever beam is carried out using eigenfrequency analysis module of the COMSOL-Multiphysics software. The dimensions measured under the electron microscope are used to model the beam. Drawn geometry is assigned same material properties as that of the real beam, and finally the simulation is performed to calculate the mode shapes and un-damped eignefrequencies of the beam. Comparison is done between analytical, computational, and experimental solutions. Figure 8.2 shows representative results of these validation which indicate excellent agreement between modeling and experimental results, which proves that the SPS_V1 does not interfere with OEHO system.

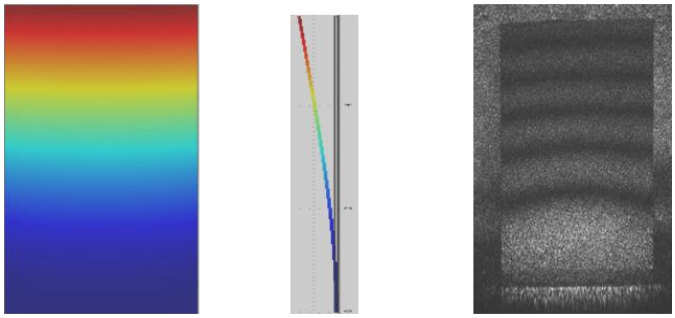

Analytical solution: 447.05 Hz
% Error: FEA w.r.t. analytical: 3%
% Error: Exp w.r.t. analytical: 5%
% Error: Exp w.r.t. FEA: 2.6%

(a)

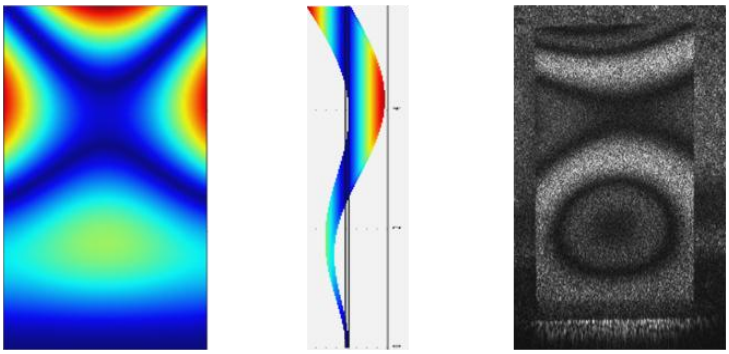

Analytical solution: 7845 Hz

% Error: FEA w.r.t. analytical: 0.3%

% Error: Exp w.r.t. analytical: 4.1%

% Error: Exp w.r.t. FEA: 4.1%

(b)

Fig. 8.2. Comparison plots of representative bending modes of vibration of a cantilever beam; (a) first bending mode, (b) second mode.

8.2. SPS_V1 performance testing in free space

As no hindrance was identified because of the SPS_V1 integration with the OEHO system, the SPS_V1 is further characterized by taking SPL measurements in its close vicinity.

As per one of the design objectives, sound field in the region up to 15 mm distance from the exit of the speculum is of prime importance. To understand the behavior of the sound field in this region of interest a virtual rectangular grid is generated. Sound pressure is measured at every node of the rectangular mesh element for the frequency range between 50 Hz and 25 kHz at a step of 50 Hz. Figure 8.3 shows the virtual mesh used to record experimental measurements of SPL.

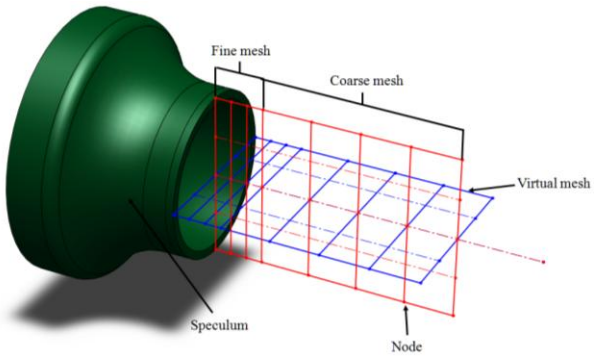

Fig. 8.3. Experimental mesh to characterize the sound field at the exit of the speculum.

The experimental mesh is created on two planes 90^o apart from each other and perpendicular to the face of the speculum. The mesh is visualized over the area of $15\ mm \times 10\ mm$. The mesh area can be divided in two main parts: fine mesh and coarse mesh. The fine mesh region, defined to observe SPL gradients, has dimensions of $3\ mm \times 10\ mm$ and it contains 20 node points. The coarse mesh region, defined to observe far field SPL gradients, has dimensions of $12\ mm \times 10\ mm$ and it also contains 20 node points.

To traverse through all the node points in the mesh region and record the sound pressure at every node, an experimental setup is realized. Three computer controlled linear stages are attached perpendicularly with one another and a microphone is mounted on top of them. The effect of mounting the linear stage perpendicular to one another, allows moving in X, Y and Z planes, which in turn enables to record sound pressure at every node. Figure 8.4 shows experimental setup that was developed for this task.

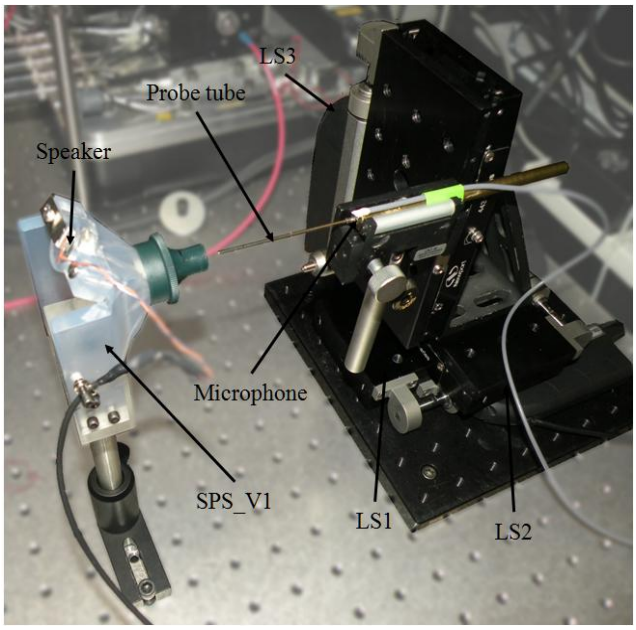

Fig. 8.4. Experimental setup to record the sound pressure at the exit of SPS_V1; LS1: linear stage allowed to move along X-axis, LS2: linear stage allowed to move along Y-axis, LS3: linear stage allowed to move along Z-axis.

To traverse the mesh region with high accuracy and to ensure that all the readings are recorded, all the linear stages are initially calibrated and then connected to a computer interface.

Before recording any readings, it is necessary to identify the origin position of the SPS_V1 with respect to probe tube microphone. To identify the origin position, initially, the tip of the probe tube is touched at four diametrically opposite points at the exit face of the speculum. Based on the readings on to the linear stages, the canter of the speculum end face is located. The center of the speculum end face serves as the origin and all the node locations are mapped with respect to the origin.

To record the sound pressure at different frequencies exact similar setup and procedures as described in Section 6.4 are implemented. The sound pressure level is recorded by taking 100 averages at an attenuation of 100 mV. All the readings are saved at the computer interface and are processed after normalizing the frequency response with the frequency response at origin, as described in Section 6.4.

8.2.1. Post-processing of free space experimental mesh readings

As the experimental mesh is made up of rectangular elements, Lagrange's polynomials are used to analyze the data and also to predict the sound pressure at intermediate locations in the rectangular element.

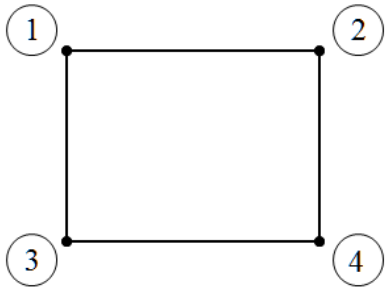

Fig. 8.5. Rectangular element of linear boundary node family.

Figure 8.5 shows a rectangular element used to compute the intermediate values of any parameter, based on the values at the nodes, viz., 1, 2, 3, and 4 [Zienkiewicz and Taylor, 1989]. Same principle is used to analyze the data recorded with the help of the experimental mesh shown in Fig. 8.3

An easy and systematic method of generating shape functions of any order can be achieved by simple products of appropriate polynomials in two co-ordinates and graphically shown in Fig. 8.6. For any given set of data points, there is only one polynomial with least possible degree that interpolates these data points.

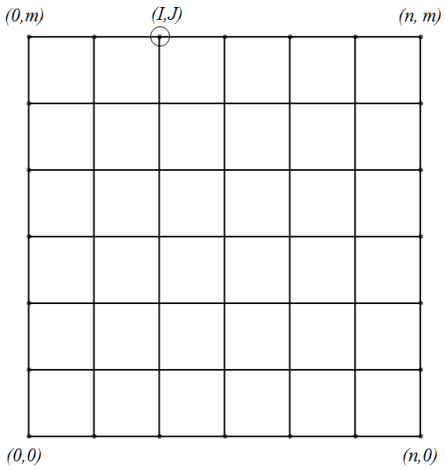

Fig. 8.6. Rectangular grid with *n+1* nodes
in *x*-direction and *m+1* nodes in *y*-direction.

For a set of $n+1$ data points in *x*- direction and $m+1$ data points in *y*-direction, where no two *xi* and *yj* are the same, the interpolation polynomial in the Lagrange form is a linear combination [Zienkiewicz and Taylor, 1989; Reddy and Gartling, 2009],

$$l_i^k(x) = \frac{(x - x_0)}{(x - x_0)} \cdots \frac{(x - x_{i-1})(x - x_{i+1})}{(x_i - x_{i+1})(x - x_{i+1})} \cdots \frac{(x - x_k)}{(x_i - x_k)} . \tag{8.2}$$

Thus, in two dimensions, if we label the node by its column and node number, *i, j,* the solution can be obtained.

Same procedure is used to plot the sound pressure distribution throughout the experimental mesh. This solution is generated using MATLAB software and illustrated in Appendix A

As the nodes in experimental mesh are really coarse when compared to computational models, the results obtained are not as smooth and uniform as in computational simulations. Cubic polynomial fit functions are used from the MATLAB software [MATLAB R2010, 2010] to obtain uniform SPL distributions. Figure 8.7 shows representative plots of sound pressure distribution in the experimental region at 1000 Hz, 4000 Hz, and 8000 Hz.

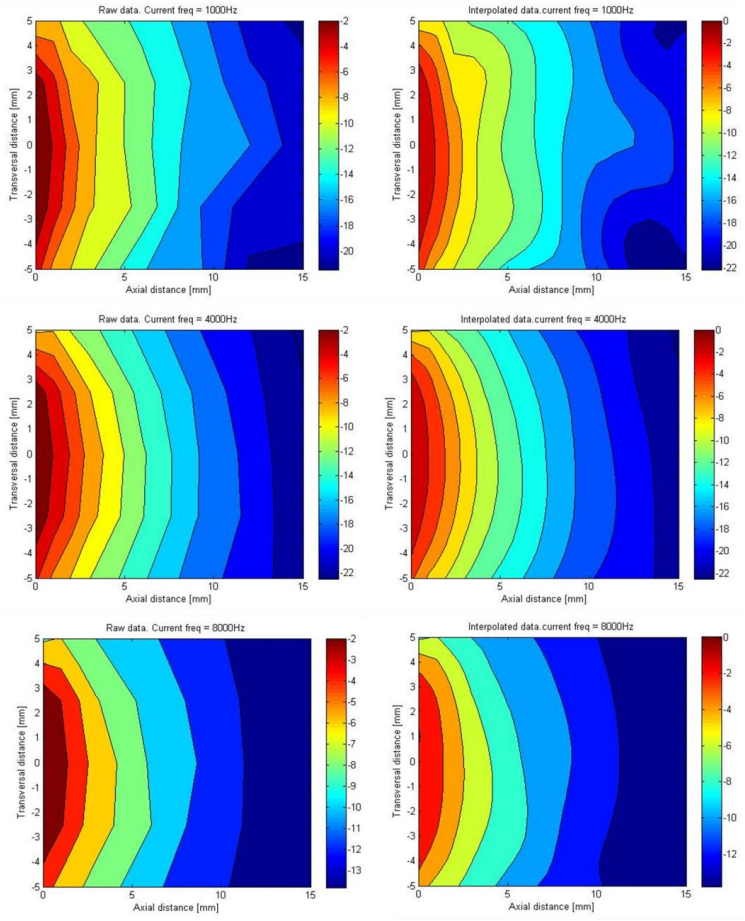

(a) (b)

Fig. 8.7. Plot of sound pressure distribution at the exit of SPS_V1 at 1kHz, 4kHz, and 8kHz (a) linear interpolation, (b) cubic interpolation.

8.3. Performance calibration in an artificial ear canal

The main objective for development of the SPS is to impinge an acoustic stimulus in the human ear in order to excite the TM (eardrum) at known frequencies so that the physical response of the TM to the acoustic stimuli can be recorded with the help of OEHO. To take these readings, it is necessary to insert the integrated package of OEHO and SPS_V1 into the ear canal.

For characterization of the SPS_V1 performance, it is necessary to investigate the effect of closed cavity on the working of the SPS_V1 [Allen et al., 2005].

To achieve this objective, a microphone with similar diameter as that of the TM is used to record the acoustic stimuli impinged towards it by the SPS_V1. The ear canal is closely simulated by using a tygon tube with dimensions of the ear canal. SPS_V1 is positioned such that the speculum tip is inserted in one end of the tygon tube while the microphone is located on the other side. Figure 8.8 shows the experimental setup used.

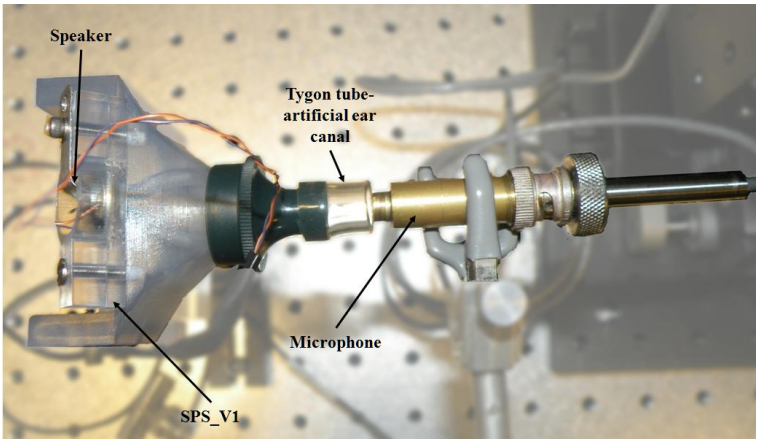

Fig.8.8. Experimental setup for characterization of SPS_V1 inside an artificial ear canal.

To achieve optimized setup of the SPS_V1 for maximum sound pressure at the TM, various possible tests are performed on SPS_V1 in combination with an artificial ear canal. These tests

include variations related to different speakers, sealing of the ear canal, sealing of the optical aperture and also number of pipes impinging the acoustic stimuli. These tests provide valuable information to understand the behavior of the system and predict the performance of SPS_V1 in real TMs.

8.3.1. 15mm diameter speaker – 3mm diameter speaker

The effect of installing two different speakers is examined by testing the SPS_V1 with a 15 mm diameter speaker and another speaker with 3 mm diameter. Representative results are shown in Fig. 8.9.

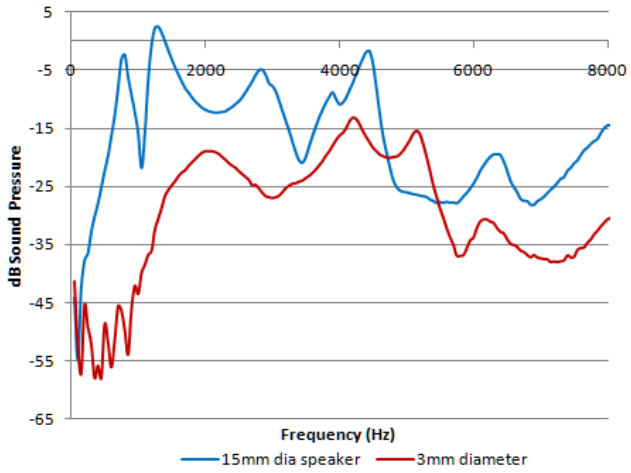

Fig. 8.9. Comparison plot of frequency response of the SPS_V1 with 15 mm diameter speaker and 3 mm diameter speaker.

8.3.2. Closed ear canal-partially open ear canal

A cavity is created inside the ear canal upon inserting SPS_V1 integrated with OEHO system in the ear canal. SPS_V1 may or may not seal the cavity from the external environment. To understand the effect of the seal on sound pressure level at the tympanic membrane, a test is carried out with completely sealed ear canal and partially open ear canal with aperture for the optical path still open, as shown in Fig. 8.10 with corresponding SPL measurements plotted in Fig. 8.11.

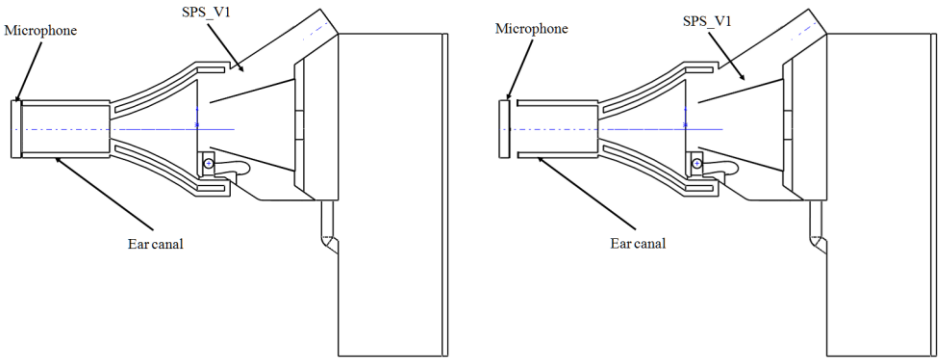

(a) (b)

Fig. 8.10. Schematic diagram of (a) Completely sealed ear canal, and (b) partially open ear canal.

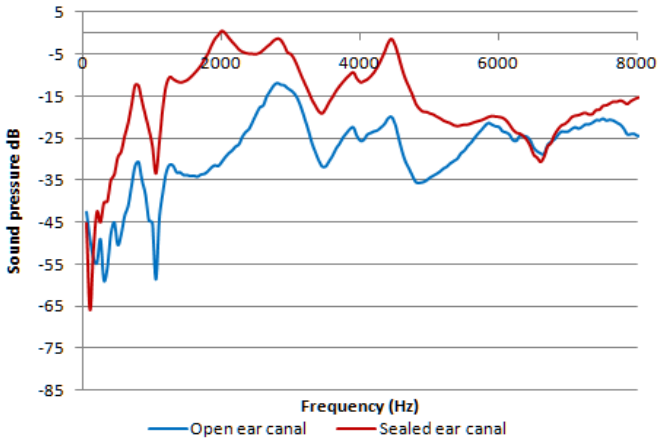

Fig. 8.11. Comparison plot of completely sealed ear canal and partially open ear canal.

8.3.3. Effect of multiple pipes carrying acoustic stimulus

To investigate the effect of using a symmetric geometry to impinge the acoustic stimuli over a non-symmetric and single pipe system, one of the pipes carrying the acoustic stimulus is blocked by a rubber adaptor inserted in it; the aperture for optical path is still open. Schematic is shown in Fig. 8.12 and representative SPL measurements recorded in Fig. 8.13.

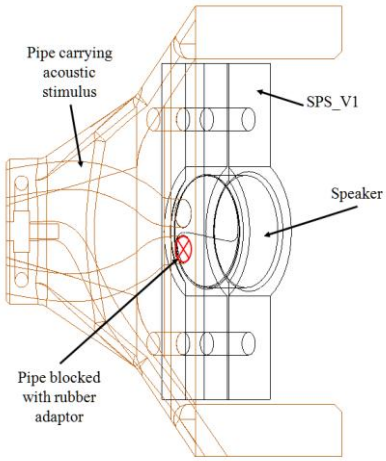

Fig. 8.12. Schematic of: (a) both pipe carrying acoustic stimulus (b) one pipe carrying acoustic stimulus.

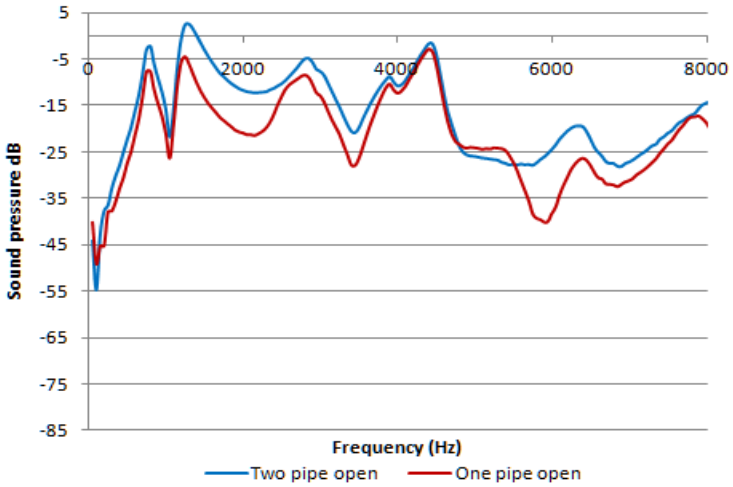

Fig.8.13. Comparison plot of frequency response of SPS_V1 with one pipe open and two pipes open.

8.3.4. Optical aperture closed – open

To examine the effect of sealing the optical aperture for sound propagation, a rubber adaptor is inserted in the optical path and the frequency response is recorded by keeping both the pipes open to carry the acoustic stimulus and sealing the ear canal completely. Same procedure is carried out without blocking the optical aperture. Schematic is shown in Fig. 8.14 and representative SPL measurements recorded in Fig. 8.15.

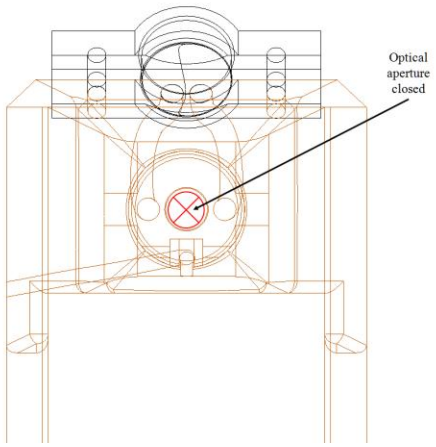

Fig. 8.14. Optical access aperture on the SPS_V1 is blocked.

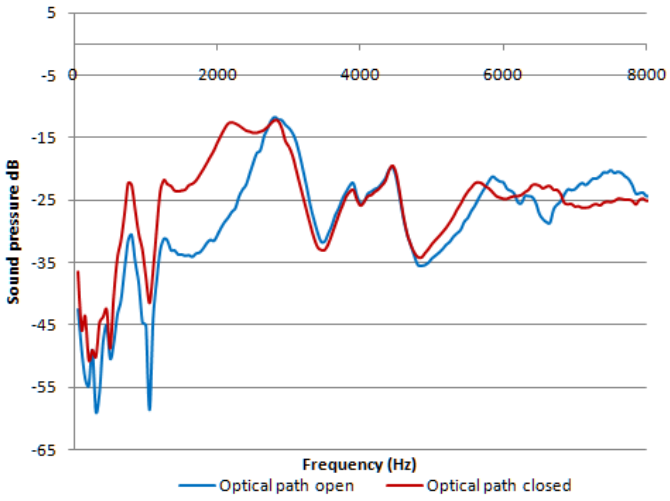

Fig. 8.15. Comparison plot of frequency response of the SPS_V1 with optical aperture open and optical aperture closed.

8.3.5. Amplitude 100mV- amplitude 320mV

The SPS_V1 was also tested for two different amplitudes of 100mV and 320mV. The ear is completely sealed, optical is path is blocked with a rubber adaptor, and both the pipes are open to carry the acoustic stimulus. Representative results are shown in Fig. 8.16.

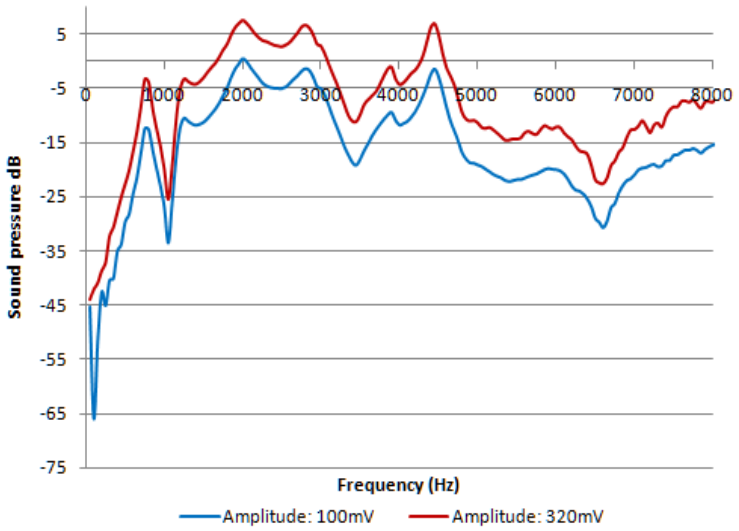

Fig.8.16. Comparison plot of frequency response of the SPS_V1 at 100mV amplitude and 320mV amplitude.

9. Conclusions and Recommendations

The principle of this thesis is to induce an acoustic stimulus through an efficient compact system integrated with OEHO for capturing comprehensive diagnostic information of the pathological conditions of the TM. The synthesized, manufactured and tested SPS_V1 design demonstrates its ability to effectively integrate with all the versions of OH systems that WPI/CHSLT labs and MEEI have developed without interfering with the optical path and by eliminating vibrations through rigidly mounted speaker. SPS_V1 also facilitates easy access to the TM by incorporating pathological speculum into its design.

Symmetric SPS_V1 design along the optical axis of the integrated system with two conduits carrying the acoustic signal exhibits enhanced potency of the sound pressure induced on the TM when compared with only one conduit carrying the acoustic signal. Higher sound pressure level achieved due to closed optical path provides useful guidelines for incorporating sealed optical path in next version of the OEHO system which would prove useful for protecting delicate optical equipment. Closed cavity formed upon inserting SPS_V1 into the ear canal reveals increased sound pressure level as compared to a partially open cavity.

Various test set ups used for efficiently selecting the optimum combination of the SPS_V1 provides definite guidelines for further development of the system. Microphone located at the front face of the SPS_V1 avoids need for additional conduit to record response from the TM. For further development of the SPS, probe the effects of damping and energy dissipation due to the pipes carrying the acoustic signal. Analyze the capacity of the system to use an array of pipes to impinge the acoustic signal on the TM. Investigate advanced software tools for correlating acoustic stimulus signal with the series of short laser pulses in stroboscopic mode.

Further miniaturization of the SPS by using MEMS technologies for selection of speaker and microphone is strongly recommended.

SPS_V1 is capable of producing more SPL than 110 dB which was a design requirement. Hence, SPS_V1 would operate satisfactorily to record holographic measurements on the TM using OEHO system at the desired frequency and the amplitude of the acoustic stimuli.

10. References

Allen, J. B., Jeng, P. S., and Levitt, H., "Evaluation of human middle ear function via an acoustic power assessment," *JRRD*, 42 (4):63-78, 2005

Bogey, C. and Bailly, C., " Three-dimensional non – reflective boundary conditions for acoustic simulations: far field formulation and validation test cases," *Acta Acustica united with Acustica*, Vol. 88, 2002

Castellini, P., Revel, G. M., and Tomasini, E. P., "Laser doppler vibrometry: A review of advances and applications," *The Shock and Vibration Digest*, 30(6):443-456, 1998

Castellini, P., Martarrelli, M., and Tomasini, E. P., "Laser doppler vibrometry: Development of advanced solutions answering to technology's needs," *Science Direct*, 20:1265-1285, 2006

Csillag, A., *Atlas of the sensory organs: functional and clinical anatomy*, 1st ed., Human press, Totowa, New Jersey, 2005

COMSOL Multiphysics, *Acoustics Module Handbook*, Burlington, MA, 2008

Dirckx, J. J., and Decraemer, W. F., "Interferometer for eardrum shape measurement based on projection of straight line rulings," *Lasers Med Sci*, 15:131–139, 2000

Edmund Optics, Inc., Edmund Optics, Inc., Barrington, NY, 2006

Egolf David P., "Mathematical modeling of a probe-tube microphone," *J. Acoust. Soc. Am.*, Vol. 61: 225-231, 1977

Fay, J., Puria. S., Decraemer, W. F., and Steele, C., "Three approaches for estimating the elastic modulus of the tympanic membrane," *J. Biomech.*, 38(9):1807-1815, 2005

Feeney, M.P., Grant, I. L., and Marryott, L.P., "Wideband energy reflectance in adults with middle-ear disorders," *Hear. Res.*, 46:901-911, 2003

Funnell, W. R., and Laszlo, C. A., "Modeling of the cat eardrum as a thin shell using the finite-element method," *J. Acoust. Soc. Am.*, 63(5):1461-1467, 1978

Furlong C., and Pryputniewicz R. J., "Hybrid computational and experimental approach for the study and optimization of mechanical components," *Opt. Eng.*, 37, 5, 1998

Furlong, C., Yokum, J. S., and Pryputniewicz, R. J., "Sensitivity, accuracy, and precision issues in opto-electronic holography based on fiber optics and high spatial and high-digital resolution cameras," *Proc. Internat. Conf*, on Measurements in Advanced Materials and Systems, Milwaukee, WI, 2002

Furlong C., Hernández-Montes, M. S., Hulli, N., Cheng, J. T., Ravicz M. E., and Rosowski J. J., "Development of an optoelectronic holographic otoscope for characterization of sound-induced displacements in tympanic membranes," *31st Midwinter Meeting of the Association for Research in Otolaryngology*, Phoenix, AZ, 2008

Grundman, J. and Wigton, R., "Tympanic membrane evaluation", in Ear Examination, online: http://webmedia.unmc.edu/intmed/general/eye&ear/introtm.html, 2010

Hernández-Montes, M. S., Furlong, C., Rosowski, J. J., Hulli, N., and Harrington, E., "Optoelectronic holographic otoscope for measurement of nano- displacements in tympanic membranes," *Proc SEM.*, 2008

Hulli N. *Development of an optoelectronic holographic otoscope system for characterization of sound-induced displacements in tympanic membranes*, M.S. Thesis, Mechanical Engineering Department, Worcester Polytechnic Institute, 2008

Katz, J., *Handbook of Clinical Audiology*, 4th ed., Williams & Wilkins, Baltimore, Maryland, 1994

Keefe, D. H., Bulen, J. C., Arehart, K. H., and Burns, E. M., "Ear-canal impedance and reflection coefficient in human infants and adults," *J. Acoust. Soc. Am.*, 94(5):2617-2638, 1993

Khanna, S. M. and Tonndorf, J.,"Tympanic membrane vibrations in cats studied by time-averaged holography," *J. Acoust. Soc. Am.*, 51(6): 1904-1920, 1972

Kinsler L., Frey A., *Fundamentals of acoustics*, Fourth edition, Wiley, 1986

Kreis, T., *Handbook of holographic interferometry*, Wiley-vch, Ch 4-5, 2005

Kuypers, L. C., Decraemer, W. F., and Dirckx J. J., "Thickness distribution of fresh and preserved human eardrums measured with confocal microscopy," *Otol. Neurotol.*, 27(2): 256-264, 2006

Lim, D. J., "Structure and function of the tympanic membrane: a review," *Acta Otorhinolaryngol.* Belg., 49(2):101-115, 1995

Li, X., Direct Solvers for Sparse Matrices, on-line: http://crd.lbl.gov/~xiaoye/SuperLU/SparseDirectSurvey.pdf, 2010

Margolis, R. H., Saly, G. L., and Keefe, D. H., "Wideband reflectance tympanometry in normal adults," *J. Acoust. Soc. Am.*, 106(1):265-280, 1999

MatLab R2010, Help, The Mathworks, Natick MA, 2010

McLachlan, N.W., *Bessel Functions for Engineers*, Oxford University Press, Amen House, London E.C.4, 1961

Mikoklai, T. K., Duffey, J., and Adlin, D., "A guide to tympanometry for hearing, on-line: http://www.maicodiagnostics.com/eprise/main/Maico/Products/Files/MI24/Guide.Tymp.pdf , 2008

Powell R. and Stetson K., "Interferometric vibration analysis by wavefront reconstruction" *J. Opt. Soc. Am.*, 55 (12): 354-359 , 1965

Pryputniewicz, R. J., "Time average holography in vibration analysis," *Opt. Eng*., 24(5): 843-848, 1985

Pryputniewicz, R. J., "Quantitative interpretation of time-average holograms in vibration analysis," *Optical metrology, in NATO Advanced Science Institute (ASI) Series*, Porto, Portugal, pp. 296-371, 1987

Pryputniewicz, R. J., "Measurement of vibration patterns using electro-optic holography," *Proc. SPIE,* 1162:456-467, 1989

Pryputniewicz, R. J., Yokum, J. S., and Furlong, C., Optoelectronic holography method for measurements of absolute inside shapes of objects, "*Proc. 2002 Internat. Conf. on Measurements in Advanced Materials and Systems*, SEM, Milwaukee, WI, 2002

Ravicz M., Olson E., and Rosowski J. J., "Sound pressure distribution and power flow within the gerbil ear canal from 100Hz to 80kHz", *J. Acoust. Soc. Am.,* 122 (4), 285-289, 2007

Rosowski, J. J., Carney, L. H, Lynch, T. J., and Peake, W. T.,"The effectiveness of external and middle ears in coupling acoustic power into the cochlea," in: *Peripheral Auditory Mechanisms,* Allen, J. B., Hall, J. L., Hubbard, A., Neely, S. T., and Tubis, A., eds, New York, Springer-Verlag, pp. 3-12, 1989

Rosowski, J. J.,"Models of external- and middle- ear function," in: *Auditory computation*, Hawkins, H. L., McMullen, T. A., Popper A. N., and Fay, R. R., eds, Springer-Verlag New York, Inc., NY, pp 15-60, 1996

Rosowski, J. J., Nakajima, H. H., and, Merchant, S. N., "Clinical utility of laser-doppler vibrometer measurements in live normal and pathologic human ears," *Ear & Hearing*, 29(1):3-19, 2008

Reddy, J. N., and Gartling, D. K., *The finite element methods in heat transfers and fluid dynamics*, CRC Press, 2009, New Jersey, 2009

Sanna, M., Sunose H., Mancini, F., Russo, A., and Taibah, A., "Middle ear and mastoid microsurgery," Georg Thierne Verlag, Stuttgart, Germany, pp.1-15, 2003

Schubert, E. D., *Hearing: Its function and dysfunction*, Springer-Verlag, New York, NY, 1980

Shanks, J. E., Lilly, D. J., Margolis, R. H., Wiley, T. L., and Wilson, R. H.,"Tympanometry," *J. Speech Hear. Dis.*, 53:354-377, 1988

Sundberg, M., *Optical methods for tympanic membrane characterization towards objective otoscopy in otitis media*, Ph. D. Dissertation, Department of Biomedical Engineering, Linköpings University, Linköping, Sweden, pp.19-21, 2008

Tonndorf, J., and Khanna, S. M.,"The role of the tympanic membrane in middle ear transmission," Ann. Otol. Rhinol. Laryngol, 79(4): 743-753, 1970

Wada, H., Kobayashi, T., Suetake, M., and Tachizaki, H., "Dynamic behavior of the middle ear based on sweep frequency tympanometry," *Audiology*., 28: 127-134, 1989

Wada, H., Ando, M., Takeuchi, M., Sugawara, H., and Koike, T., "Vibration measurement of the tympanic membrane of guinea pig temporal bones using time averaged speckle pattern interferometry," *J. Acoust. Soc. Am.*, 111(5): 2189-2199, 2002

Welch Allyn Inc., *Welch Allyn Digital Macroview Otoscope*, Arlington, TX, 2010

Wikipedia, "Anatomy of the human ear: The cross section of human ear showing divisions of the outer, middle, and inner ears," on- line: http://en.wikipedia.org/wiki/Eardrum, 2011

Zienkiewicz, O.C., and Taylor, R. L., *The finite element method*, Fourth edition, Vol. 1, London, McGraw Hill, 1989

Appendix A – COMSOL Multiphysics acoustic problem simulation procedure

A step by step procedure for configuration and analysis of generalized acoustic problem simulation is demonstrated in this section.

1. Start COMSOL Multiphysics software, select space dimension: 3D, Expand acoustic module domain.

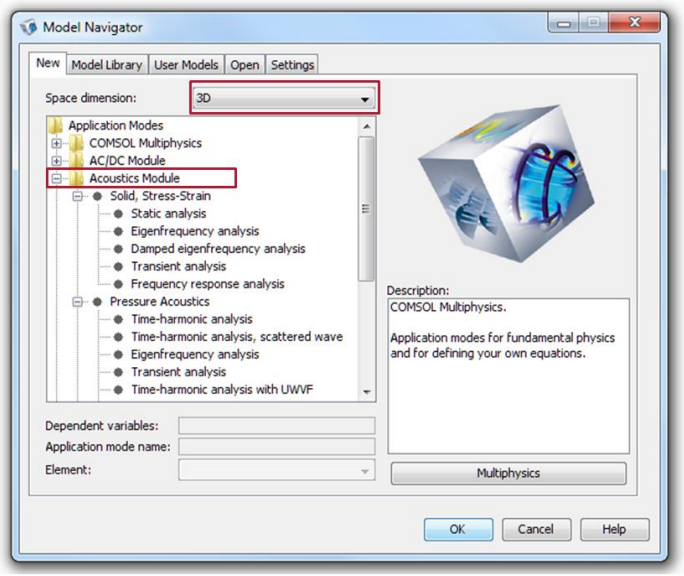

2. Expand Solid, stress-strain and Pressure acoustic module, select frequency response analysis and time harmonic analysis from subsequent modules. Modify Dependent variables and element type based on problem requirement. Click on multiphysics and add both the modules to the problem.

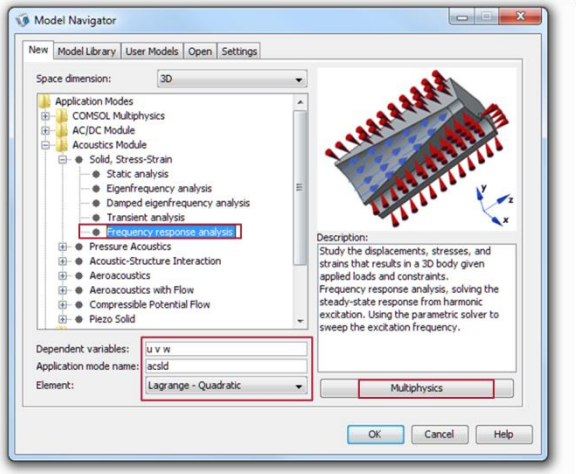

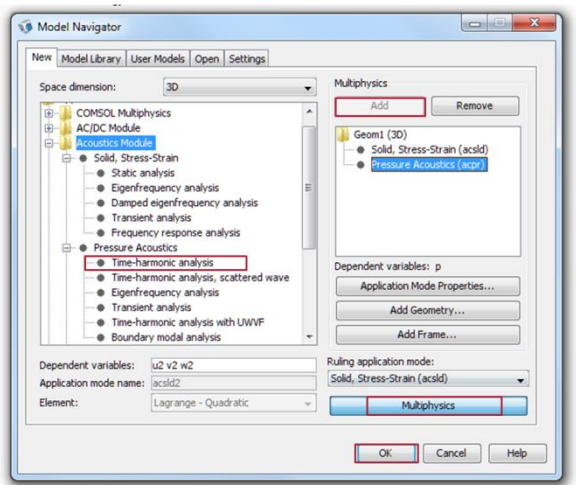

3. The problem solving method for ant simulation is from right to left in COMSOL multiphysics software. Starting from defining constants, drawing geometry, defining physics, generating mesh, solving the problem and post processing.

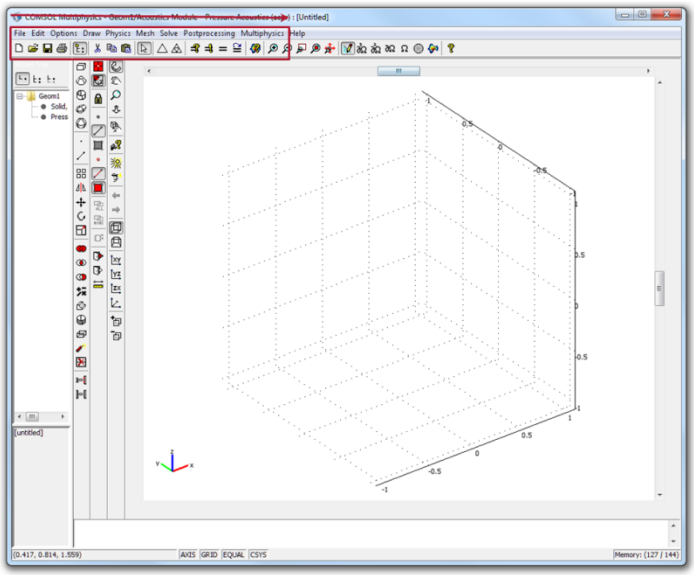

4. To define constants required for solving the problem, go to options, select constants. Insert all the constants with uints in the blank dialog box.

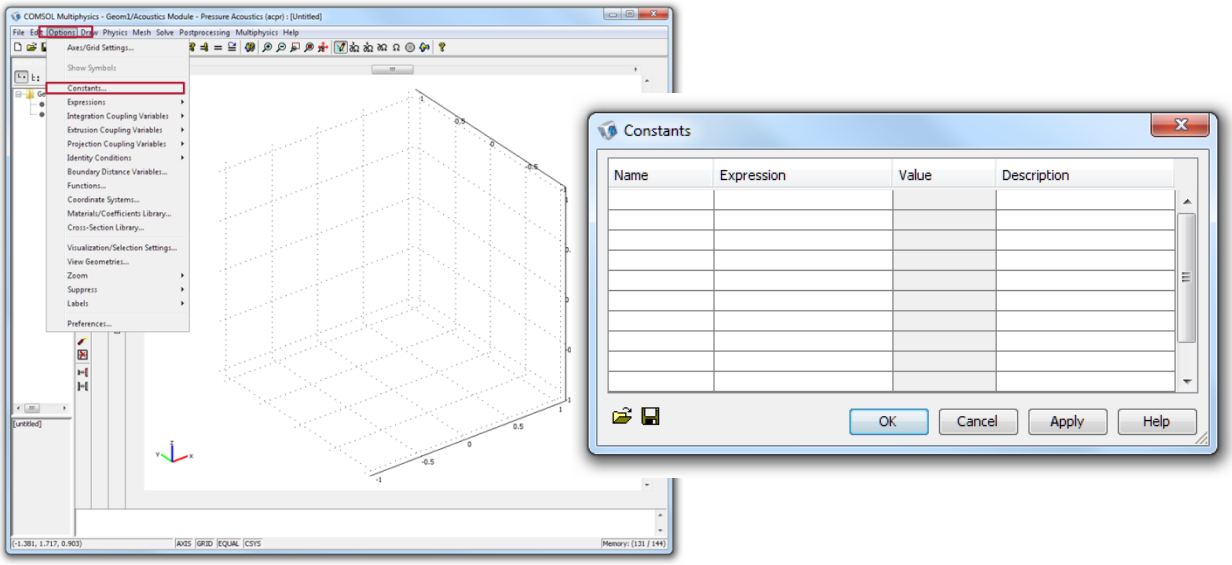

5. Depending on the complexity of the problem, geometry can be drawn in COMSOL Multipysics or CAD model can be imported in the form of IGES file. Go to Draw, select required geometry and enter coordinates and dimensions to create strucutral model.

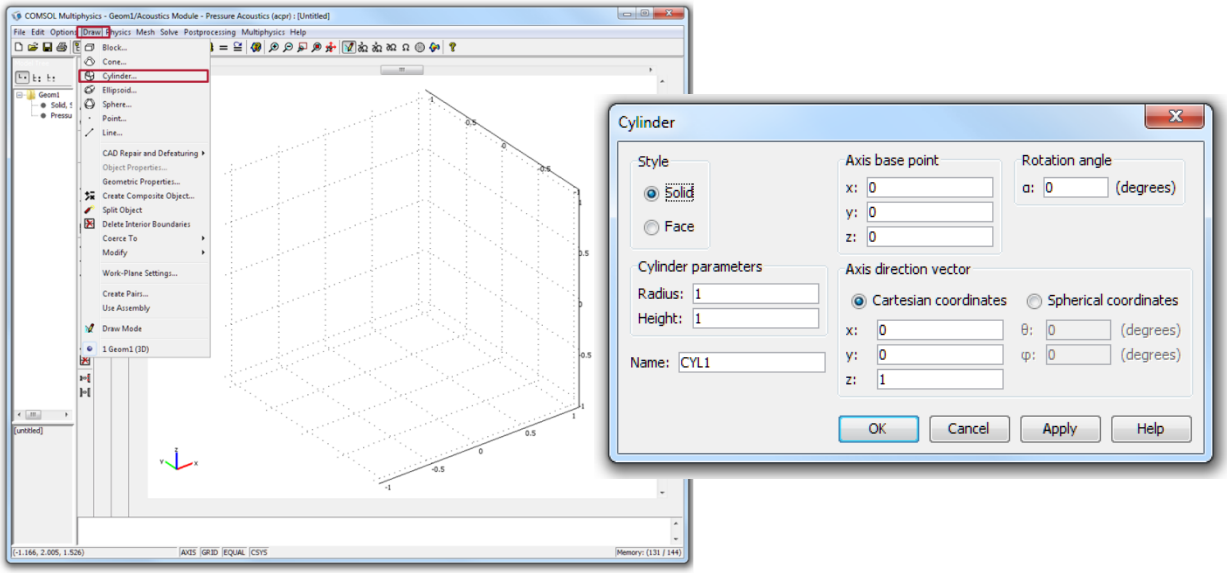

6. To define parameters depending on specific multiphysics. Go to multipysics and select pressure acoustics. Go to physics and select sub-domain settings.

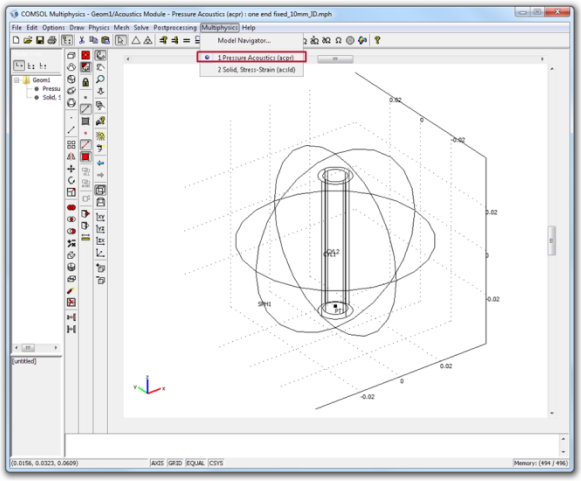

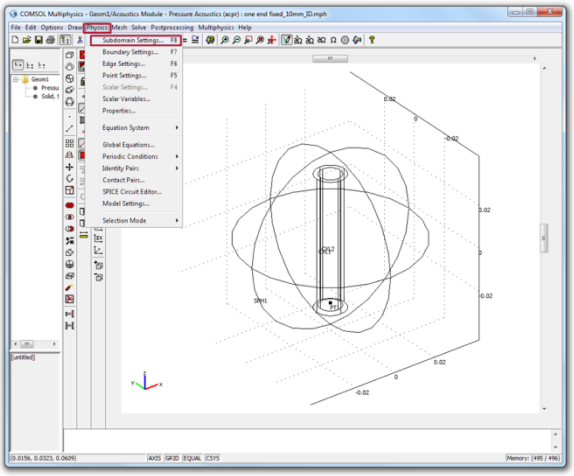

7. Selecting Sub-domain settings would prompt a dialog box to problem specifications. Top of the dialog box shows principal equation used. Entire drawn or imported geometry is divided in subdomains. Select necessary subdomains and apply appropriate Sub-domain settings.

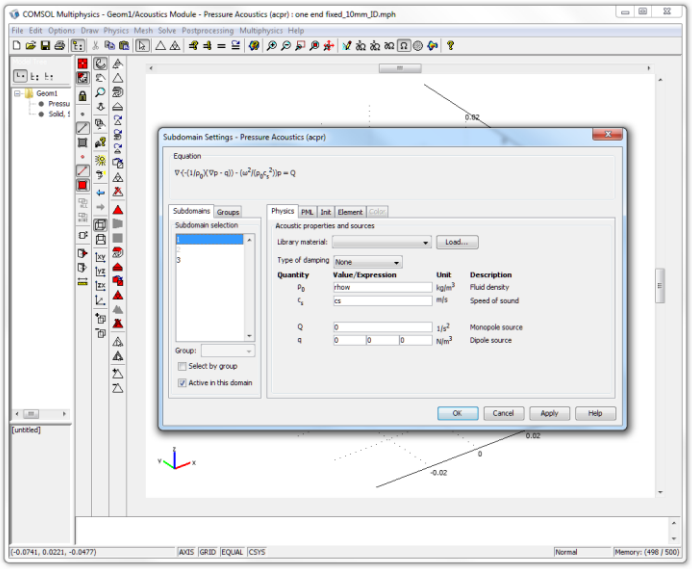

8. To assign boundary settings go to physics and select boundary settings. A dialog box would open enlisting all the element boundaries in the model drawn. Select appropriate boundary to apply necessary boundary conditions.

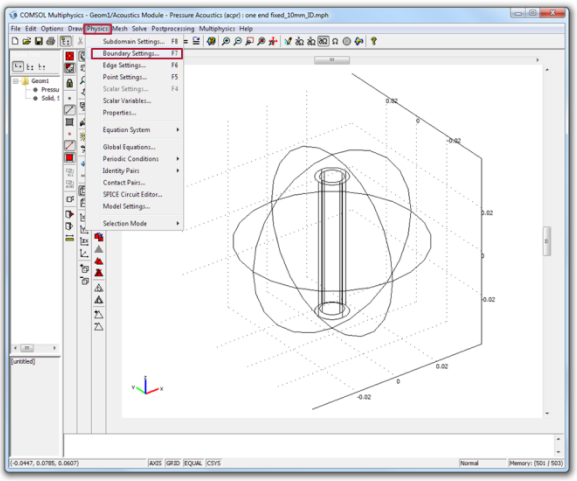

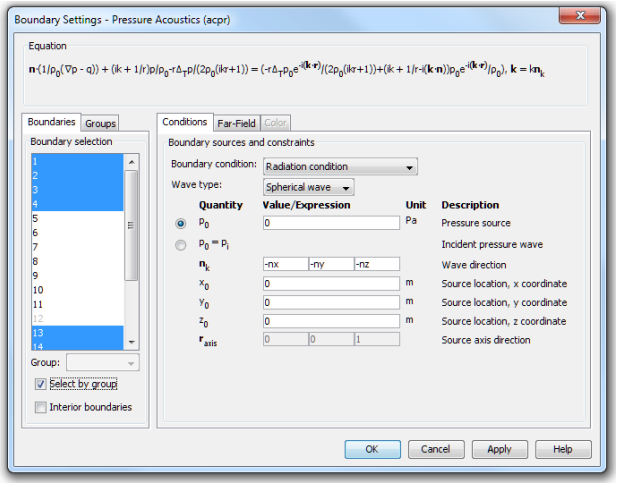

9. If point settings are required to be defined, go to physics and select point settings. Enter specifications in the point settings dialog box.

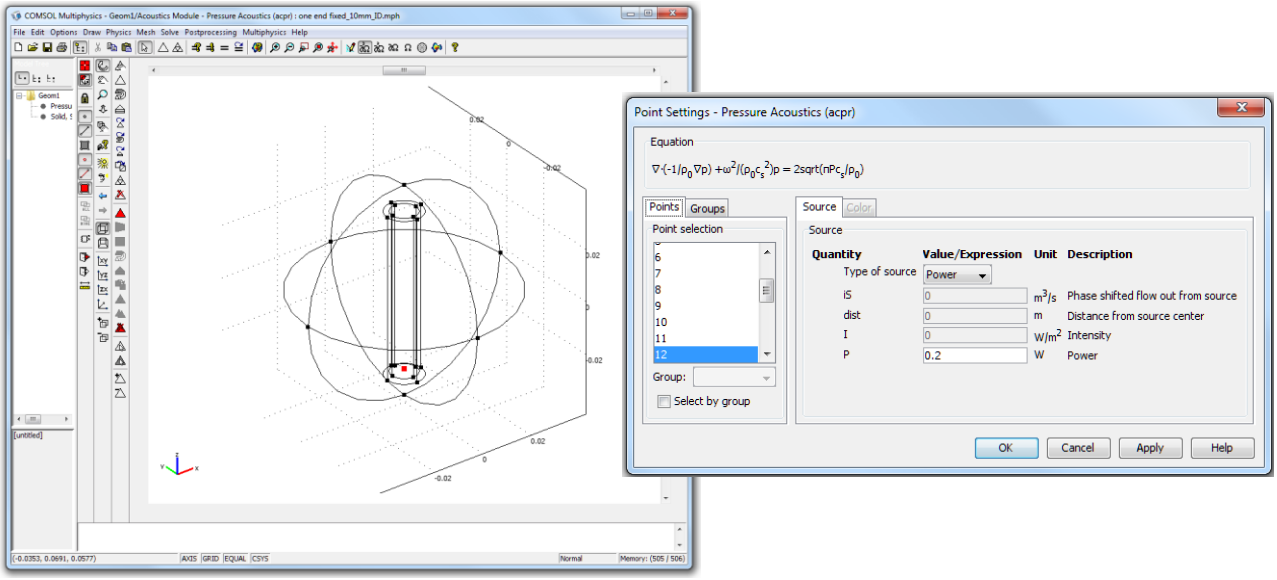

10. To account for multiphysics problems, Go to multiphysics, select solid, stress-strain module.

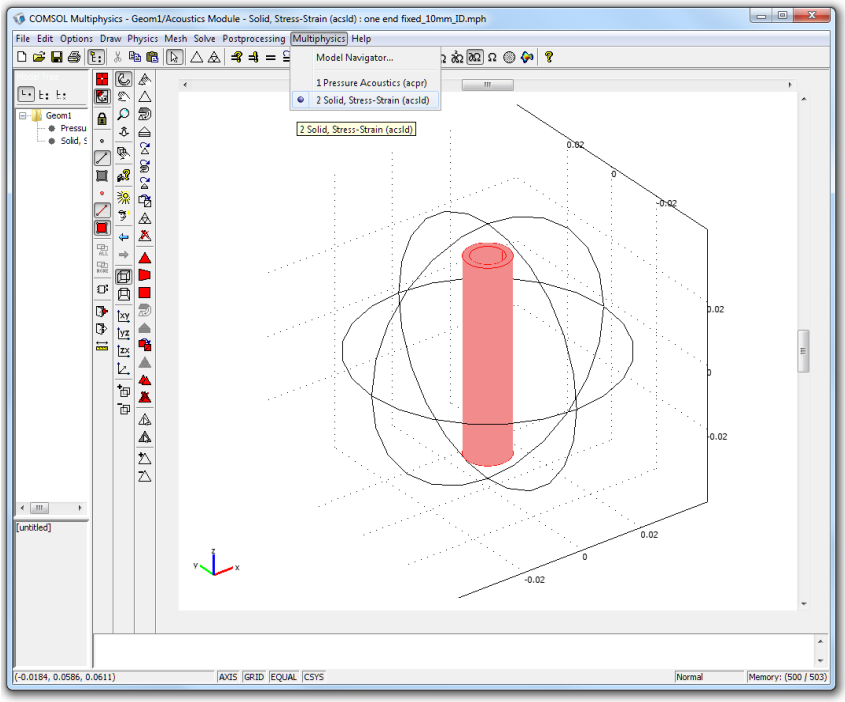

11. As required by the complexity of the problem and modules selected at the start of the simulation, similar to first module, define sub-domain settings and boundary conditions for every additional module. COMSOL multiphysics carries vast material library. Necessary material can be selected from the library or specific material properties can be entered if required.

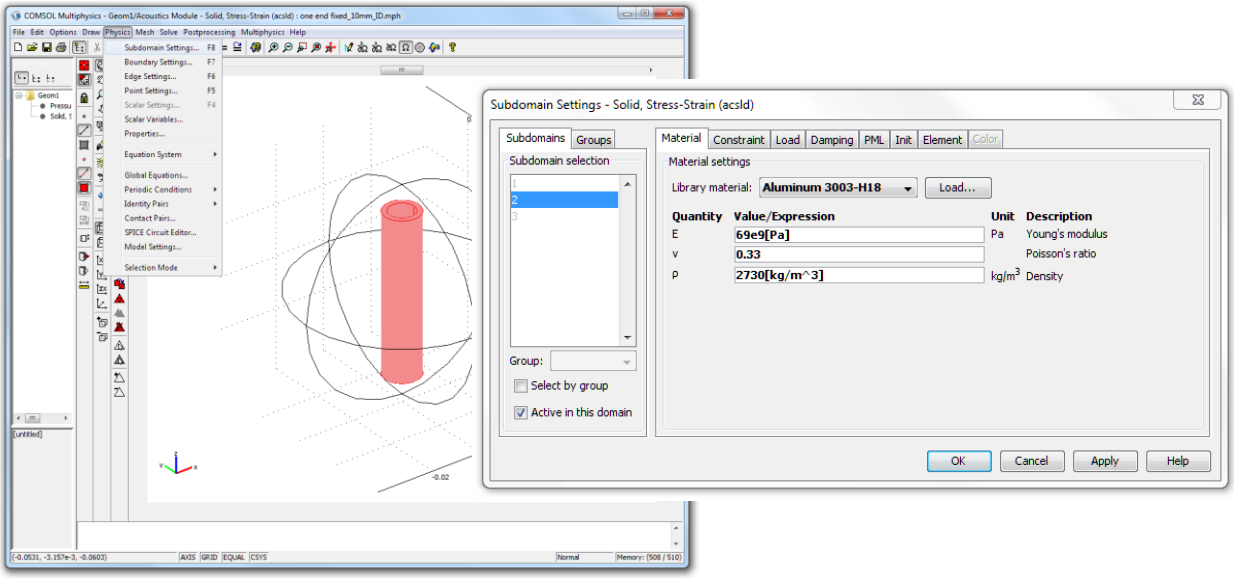

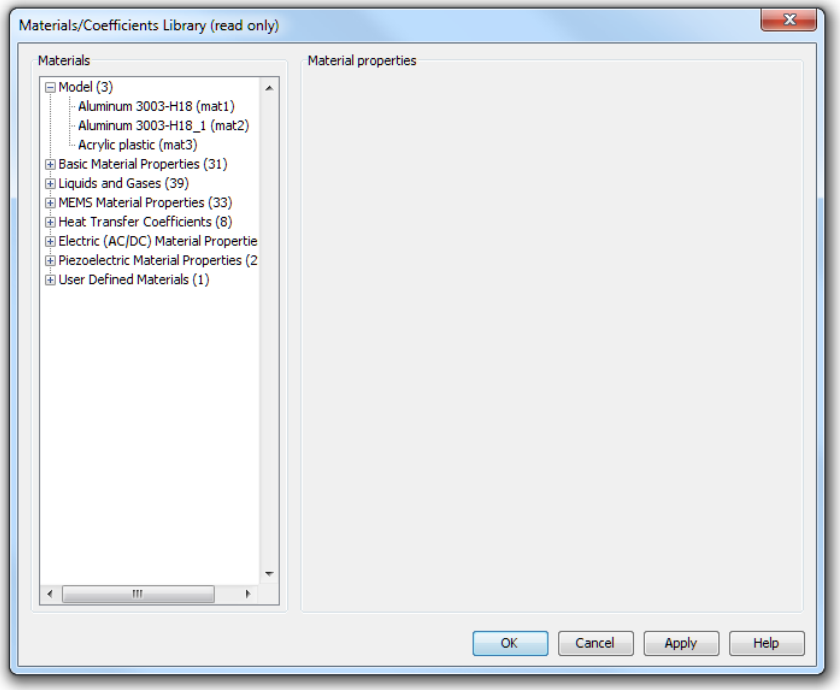

12. To generate the mesh go to Mesh, select free mesh parameter, select customer mesh size, enter maximum element size depending on the frequency range of the problem to be solved. For consistent results COMSOL multiphysics requires minimum 6 waves assigned for every frequency. To assign specific mesh size for specific sub-domains, select sub-domain tab from mesh dialog box.

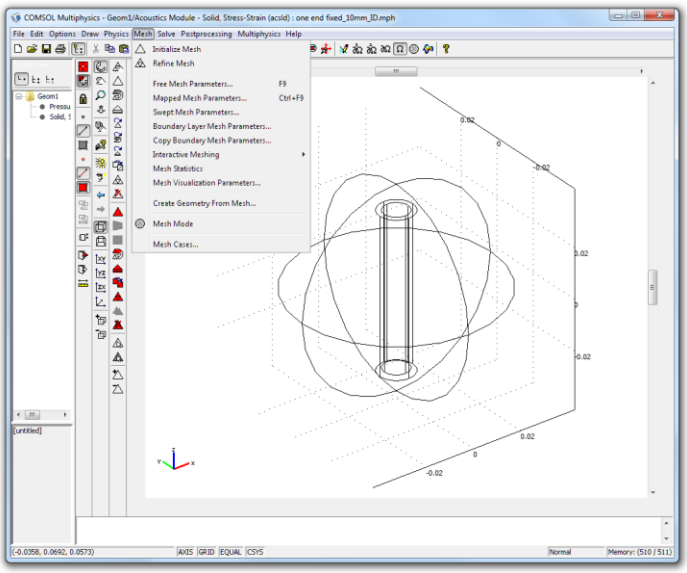

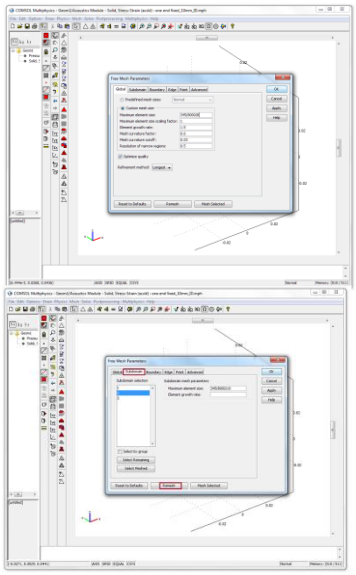

13. Upon selecting mesh parameters, select remesh to generate mesh for the simulation.

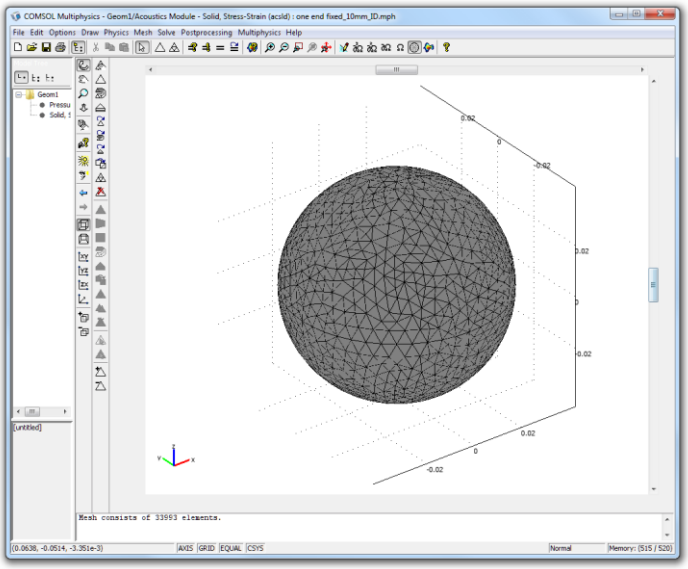

14. To solve the problem select solver parameters, in solver parameter dialog box input parameters starting from analysis type, solver specification, type name of the parameter defined in constants box in ‘parameter names’, to define parameter range click on ‘edit’ and enter range with step size. Click ok and press ‘=’ sign to start the simulation.

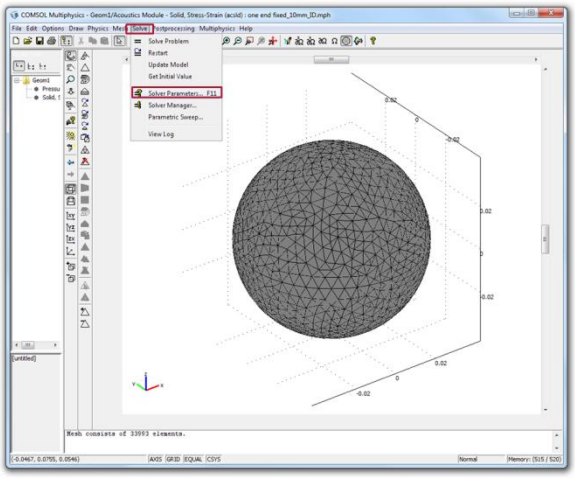

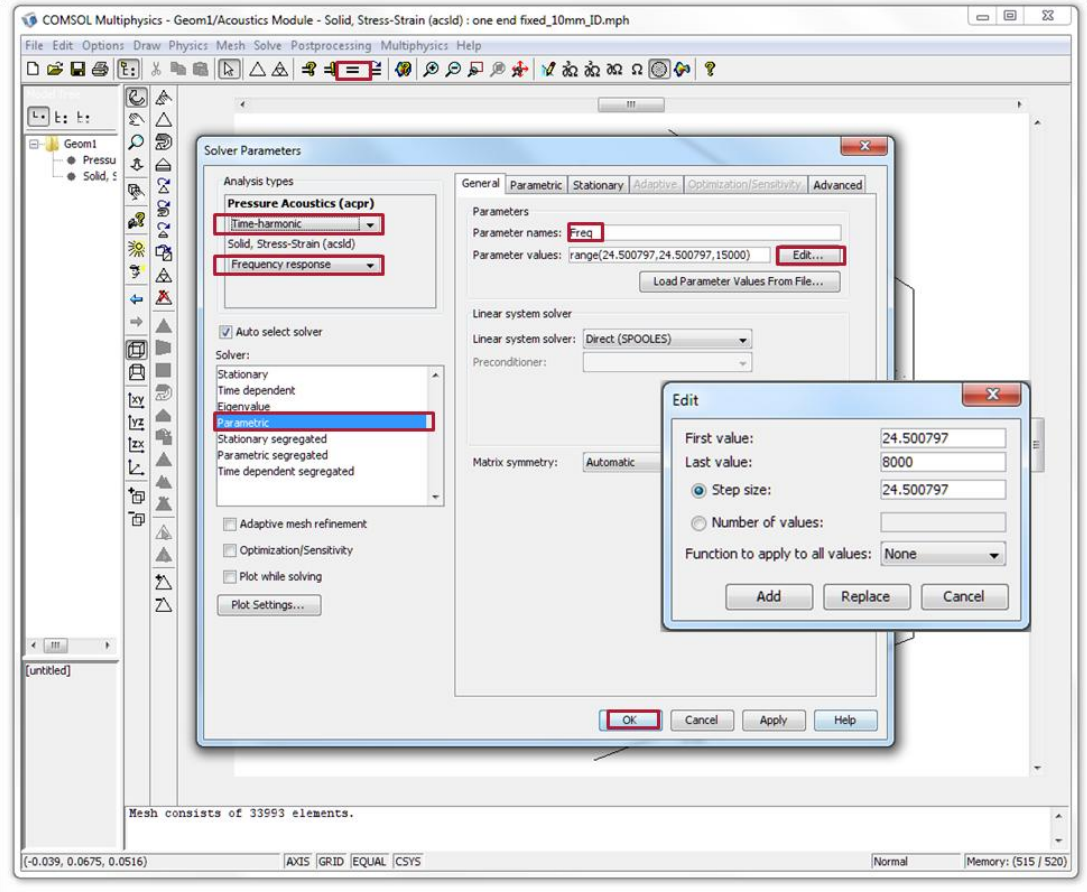

15. To analyze the result of simulation select post processing. In the dialog box either select specific parameter value or multiple values by pressing ctrl. Select type of plot and click ok.

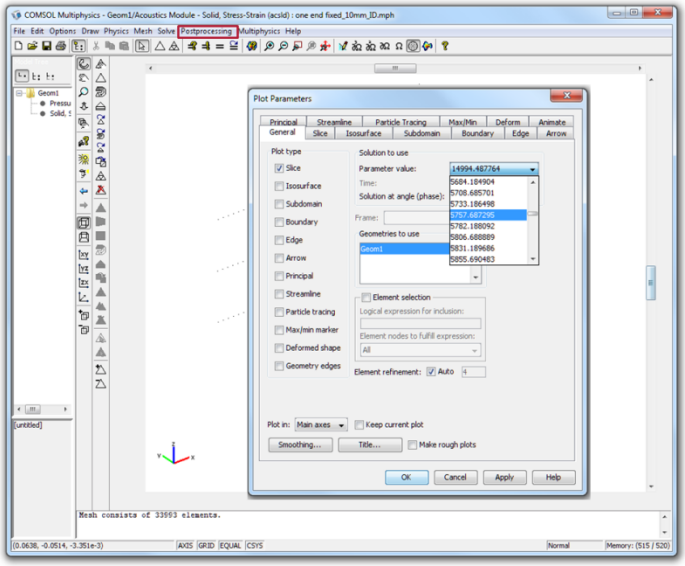

16. To create slice plot in any plane of the geometry simulated select slice tab, define plane coordinates, select predefined quantities and click ok.

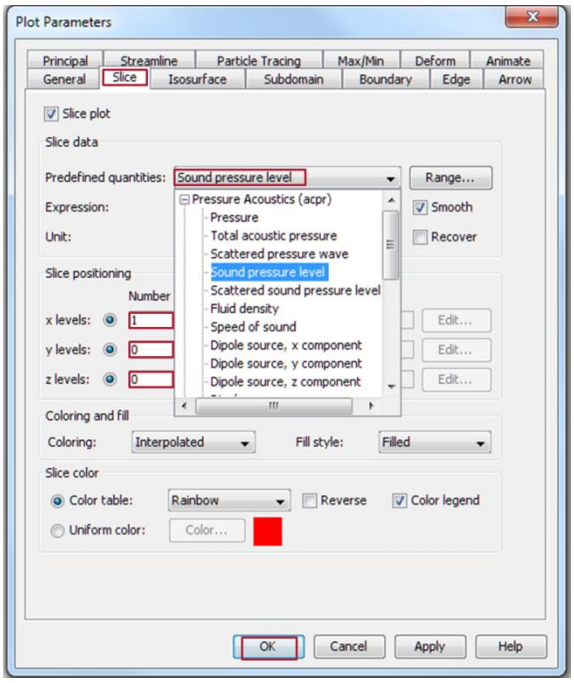

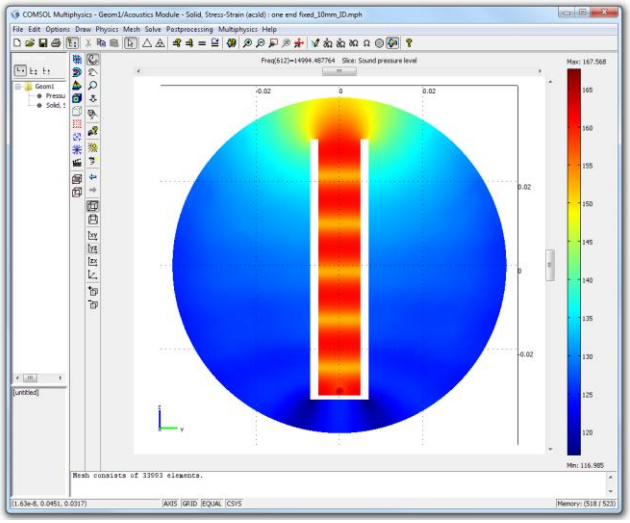

Appendix B – MATLAB Program to plot free space experimental mesh readings

```
%% Initialization variables
clear all; clc;close all;

%% Data range and location

%Upper and lower border of file name range variables
number_range_min = 1;
number_range_step = 1;
number_range_max = 80;
number_range = number_range_min:number_range_step:number_range_max;
number_range_size = size(number_range,2);

mesh_width = 5;
mesh_lengh = 8;
plane_data_size = 40;

XY_plane_data = 1:40;
XZ_plane_data = 41:80;

%location of the files
location ='C:\Nikhil\Thesis\analytical\Acosutsic tests of Human
Holog\100430\';
spacial_coordinates ='C:\Nikhil\Thesis\analytical\Acosutsic tests of Human
Holog\100430\Spacial_coordinates.txt';

%fucntion for creating names out of numbers
num2name=@(number)IntToStr(number,location);


%% test
%str iterator for the names of the files
str_name=num2name(1);


delimiter = '\t';
%read only from 500Hz to the end
headerlines = 17;



newData = importdata(str_name, delimiter, headerlines);
rawData = newData.data;
Amp = rawData(:,2);

%% initialize

%read positional infomation
```

```
XYZ_raw = importdata(spacial_coordinates,delimiter);
XYZ_size = size(XYZ_raw,1);

%extract cartesian positions
X = XYZ_raw(:,2);
Y = XYZ_raw(:,3);
Z = XYZ_raw(:,4);

%freq range
freq = 500:50:25000;

%size of data
data_size = size(Amp,1);

Amp_distribution = zeros(plane_data_size,data_size);

%% Extract all data


    for number = 1:plane_data_size;

        str_name=num2name(XY_plane_data(1,number));

        newData = importdata(str_name, delimiter, headerlines);
        rawData = newData.data;

        Amp = rawData(:,2);

        Amp_distribution(number,:)=Amp(:,1);

    end

%% Group and sort
% Full_data_XY =
[X(XY_plane_data,1),Y(XY_plane_data,1),Amp_distribution(XY_plane_data,1)];
%
% Full_data_XY_sorted = sortrows(Full_data_XY,[1 2]);

%% de-mess
x_full = zeros(mesh_lengh,mesh_width);
y_full = zeros(mesh_lengh,mesh_width);
A_full = zeros(mesh_lengh,mesh_width,data_size);

%remapping from experimental orientation of the data to mesh orientation.
for i = 1:plane_data_size

    j = floor((i-1)/5)+1;%magic
    k = Y(i,1)/(2.5)+3;

    x_full(j,k) = X(i,1);
    y_full(j,k) = Y(i,1);
    A_full(j,k,:) = Amp_distribution(i,:);
end
```

```
%% interpolate
%create new(finner) mesh for the interpolation fucntion
[X_new,Y_new] = meshgrid(0:1:15,-5:.5:5);

%desired freq to test
desired_freq = 11;

%extract frequency responce of the nose
origin_scaling =  Amp_distribution(3,:);
%extract amplitude of all points at 500Hz
A_full_base_freq = A_full(:,:,1);

%raw data at desired freq
A_full_one_freq = A_full(:,:,desired_freq);
%Normalize by the pressure at the center **********************************
A_full_one_freq= A_full_one_freq-
A_full_one_freq(1,3);%**********************

%scale wrt to the responce at the nose at the desired freq
%A_full_one_freq_scaled = A_full_one_freq_norm -
origin_scaling(1,desired_freq);



%interpolate data using cubic interpoation with the X_new,Y_new as new mesh
Z_new = interp2(x_full',y_full',A_full_one_freq',X_new,Y_new,'cubic');

%plot raw data
figure(1);
contourf(x_full,y_full,A_full_one_freq)
title(['Raw data. Current freq = ',num2str(freq(desired_freq)),'Hz']);
ylabel('Transversal distance [mm]')
xlabel('Axial distance [mm]')
zlabel('Sound pressure [dB]')
colorbar

%plot interpolated data
figure(2);
subplot(2,1,1)
contourf(X_new,Y_new,Z_new)
title(['Interpolated data.current freq =
',num2str(freq(desired_freq)),'Hz']);
ylabel('Transversal distance [mm]')
xlabel('Axial distance [mm]')
zlabel('Sound pressure [dB]')
colorbar

subplot(2,1,2)
contour(X_new,Y_new,Z_new);
title(['Countour plot of interpolated data. Current freq =
',num2str(freq(desired_freq)),'Hz']);
ylabel('Transversal distance [mm]')
```

```
xlabel('Axial distance [mm]')
zlabel('Sound pressure [dB]')
h = legend(['Countour plot of interpolated data. Current freq =
',num2str(freq(desired_freq)),'Hz']);
set(h,'Interpreter','none')
colorbar
%%
% nframes = number of frames in movie
nframes=490;
M1=moviein(nframes);
M2=moviein(nframes);

figure(3);
% Note: memory can be reduced by making the plot window smaller
% and commands to get and set the current plot size are...
% get(gca,'Position')
% set(gca,'Position',[0.1 0.1 0.8 0.8]);
% loop to produce frames of the movie (frames stored in matrix M)



for it=1:nframes

    desired_freq = it;


   %raw data at desired freq
A_full_one_freq = A_full(:,:,desired_freq);
%Normalize by the pressure at the center **********************************
A_full_one_freq= A_full_one_freq-
A_full_one_freq(1,3);%**********************

%scale wrt to the responce at the nose at the desired freq
%A_full_one_freq_scaled = A_full_one_freq_norm -
origin_scaling(1,desired_freq);



%interpolate data using cubic interpoation with the X_new,Y_new as new mesh
Z_new = interp2(x_full',y_full',A_full_one_freq',X_new,Y_new,'cubic');


    %plot interpolated data
    contourf(X_new,Y_new,Z_new);
    view(0,-90);
    title(['Countour plot of interpolated data. Current freq =
',num2str(freq(desired_freq)),'Hz']);
    ylabel('Transversal distance [mm]')
    xlabel('Axial distance [mm]')
    zlabel('Sound pressure [dB]')
    colorbar
    %h = legend(['Countour plot of interpolated data. Current freq =
',num2str(freq(desired_freq)),'Hz']);
    %set(h,'Interpreter','none')
```

```
drawnow;
pause(0.01);
M1(:,it)=getframe;
end;

%% play movie
% various commands to show movie
figure(5);
movie(M1);
%movie(M,3);

 %% save movie

  movie2avi(M1, 'movie_test4.avi','fps',15)
```